國立臺灣大學生命科學院生命科學系
博士論文

Department of Life Science
College of Life Science
National Taiwan University
Doctoral Dissertation

斑馬魚Pax1a和Pax1b調控咽囊形態形成與角鰓軟骨發育之研究

Function of Zebrafish Pax1a and Pax1b in pharyngeal pouch morphogenesis and ceratobranchial cartilage development

劉昱秀

Yu-Hsiu Liu

指導教授：黃聲蘋 博士

Sheng-Ping L. Hwang, Ph.D.

中華民國 109 年 4 月
April, 2020

doi:10.6342/NTU202000783

國立臺灣大學博士學位論文
口試委員會審定書

斑馬魚 Pax1a 和 Pax1b 調控咽囊形態形成與角鰓軟骨發育之研究

Function of Pax1a and Pax1b in pharyngeal pouch morphogenesis and ceratobranchial cartilage development

本論文係劉昱秀君（學號 D00B41004）在國立臺灣大學生命科學學系、所完成之博士學位論文，於民國 109 年 4 月 15 日承下列考試委員審查通過及口試及格，特此證明

口試委員：

__________（簽名）
（指導教授）

__________ __________

__________ __________

生命科學系 系主任 黃偉邦（簽名）

誌謝

感謝指導教授黃聲蘋博士讓我進入分子生物的領域，在我的研究生涯耐心仔細的指導與教誨並給予無限的包容與體諒，在發表期刊與撰寫論文時不厭其煩地斧正及修改英文，衷心感謝老師。

感謝口試委員胡清華博士、李士傑博士、管永恕博士及王文德博士於百忙之中參與論文審查匡正疏漏並惠賜卓見，獻上衷心的感謝。

感謝在 R106 實驗室相遇的宜群學長、阿斌學長、哲毅、怡禎、銘原、小賴、芳琪、坤陽、儀婷、立瀚、人杰、子琪、彥伶、之皓、慈盈、健脩、自君、瑋銓，懷念一起度過的做實驗、討論、吃喝玩樂時光。

感謝照顧斑馬魚的阿香姊、莉穎姊、美貞姊。

感謝現在還在實驗室一起生活一起忙碌的玉芬和湘羚，可以討論實驗也能聊生活大小事，有你們增添了實驗室的色彩和歡樂，特別感謝實驗巧手玉芬還有常常陪我聊天的美貞姊。

感謝細生所共儀的杜杜和紹君教導我操作儀器，and thank Macus for editing my paper.

感謝身為做研究的前輩常常關心我給我建議和討論的宣慶學長、周銘翊學長和柏凱學長。

感謝冉繁華老師和實驗室的舊戰友阿威、Bobi、子渝、小綠、協峻…

感謝好朋友們佳祺、珮宜、偉微、宗緯、阿傑、馥宇，陳年老友子霈和怡樺，還有室友兼好友淳繡，感謝一路的相伴與支持。

謝謝玉軒(而不是梁靜茹)給了我面對挫敗和壓力的勇氣。

感謝無法計數的斑馬魚的犧牲。

最後感謝親愛的家人，一直以來的支持與愛，讓我懂得欣賞世界的美好常懷感恩的心，也從沒給我什麼壓力，還做我的後盾，讓我任性自由的活著之外還能想著盡一己之力為周遭付出。

doi:10.6342/NTU202000783

摘要

咽弓 (pharyngeal arches) 是由三個胚層所衍生的結構，且其組織間的分子相互作用是之後咽軟骨正常發育所必需的。然而，此過程的基礎機制尚未完全釐清。這篇論文主要報導斑馬魚 Pax1a 和 Pax1b 在咽囊形態形成和隨後的角鰓軟骨 (ceratobranchial cartilage) 發育中具有重疊與不可或缺的功能。 *pax1a* 和 *pax1b* 共同表現在咽囊中，運用增強子捕獲所產生的 *Tg（pax1b：eGFP）*螢光魚進行延時攝影影像觀察進一步揭示了咽囊發育的連續性分節情形。由 CRISPR-Cas9 誘變產生的 *pax1a*$^{-/-}$; *pax1b*$^{-/-}$雙突變斑馬魚胚胎的咽囊 2-5 無分節，囊狀外凸 (outpocketings) 變小。受精後 36 小時（hpf）雙突變斑馬魚胚胎的咽囊 2-5 中也沒有 *fgf3*，*tbx1* 和 *edn1* 在內胚層表現。在受精後 96 或 36 小時的 CRISPR 突變魚胚胎與以反義嗎啉基(antisense morpholino)弱化斑馬魚 *pax1a* 和 *pax1b* 基因的胚胎中，觀察到角鰓軟骨 1-4 的消失以及在咽弓 3-6 中 *dlx2a* 和 *hand2* 表現的減少或缺乏。這些結果顯示斑馬魚 Pax1a 和 Pax1b 透過調節 *fgf3* 和 *tbx1* 的表現來調節咽囊的形態形成。此外，我們的數據支持一個假說:內胚層表現的 Pax1a 和 Pax1b 蛋白質透過 Fgf3 和 Tbx-Edn1 訊號傳導，經由調控 *dlx2a* 和 *hand2* 的表現來非自主性地調節角鰓軟骨的發育。

關鍵詞：Pax1a 蛋白質、Pax1b 蛋白質、斑馬魚、咽弓、咽囊、*fgf3* 基因、*tbx1* 基因

doi:10.6342/NTU202000783

Abstract

Pharyngeal arches are derived from all three germ layers and molecular interactions among the tissue types are required for proper development of subsequent pharyngeal cartilages; however, the mechanisms underlying this process are not fully described. Here we report that in zebrafish, Pax1a and Pax1b have overlapping and essential functions in pharyngeal pouch morphogenesis and subsequent ceratobranchial cartilage development. Both *pax1a* and *pax1b* are co-expressed in pharyngeal pouches, and time-lapse imaging of a novel *Tg*(*pax1b:eGFP)* enhancer trap line further revealed the sequential segmental development of pharyngeal pouches. Zebrafish *pax1a*$^{-/-}$; *pax1b*$^{-/-}$ double mutant embryos generated by CRISPR-Cas9 mutagenesis exhibit unsegmented pharyngeal pouches 2-5 with small outpocketings. Endodermal expression of *fgf3*, *tbx1* and *edn1* is also absent in pharyngeal pouches 2-5 at 36 hours post fertilization (hpf). Loss of ceratobranchial cartilage 1-4 and reduced or absent expression of *dlx2a* and *hand2* in the pharyngeal arches 3-6 are observed in CRISPR mutant and morphant embryos that are deficient in both zebrafish *pax1a* and *pax1b* at 96 or 36 hpf. These results suggest that zebrafish Pax1a and Pax1b both regulate pharyngeal pouch morphogenesis by modulating expression of *fgf3* and *tbx1*. Furthermore, our data support a model wherein endodermal Pax1a and Pax1b act through Fgf3 and Tbx-Edn1 signaling to non-autonomously regulate the development of ceratobranchial cartilage

doi:10.6342/NTU202000783

via expression of *dlx2a* and *hand2*.

Keywords: Pax1a, Pax1b, Zebrafish, Pharyngeal pouch, Pharyngeal arch, *fgf3*, *tbx1*

doi:10.6342/NTU202000783

目　錄

口試委員會審定書…… I

誌謝…… II

中文摘要…… III

Abstract…… IV

1. Introduction…… 1

1.1 Craniofacial structure of zebrafish…… 1

1.2 Neural crest morphogenesis…… 3

1.3 Pharyngeal dorsoventral patterning…… 7

1.4 Requirement of endoderm for craniofacial cartilage formation..... 8

1.5 Pax1…… 14

1.6 The specific aims of this thesis…… 18

2. Materials and Methods…… 20

2.1 Zebrafish strains and husbandry…… 20

2.2 Generation of *Tg(pax1b:eGFP)* enhancer trap transgenic fish…. 20

2.3 Generation of *pax1a* mutants and *pax1b* mutants via CRISPR-Cas9 genome editing system and off-target analysis…… 21

2.4 Morpholino-mediated knockdown…… 23

2.5 Construction of *pax1a*-eGFP and *pax1b*-eGFP for testing MO knockdown specificity…… 24

2.6 mRNA synthesis, *in situ* hybridization, immunofluorescence and

doi:10.6342/NTU202000783

TUNEL…… 25

2.7 Alcian blue staining…… 28

2.8 Chromatin immunoprecipitation…… 28

2.9 Semi-quantitative reverse-transcription polymerase chain reaction (RT-PCR) and Real-time quantitative reverse-transcription polymerase chain reaction (RT-qPCR)…… 31

2.10 Western blot…… 34

2.11 Paraffin section…… 36

2.12 Image acquisition, statistics, and quantification of area…… 36

3. Results…… 38

3.1 zebrafish *pax1a* and *pax1b*…… 38

3.2 *pax1a* and *pax1b* are co-expressed in pharyngeal pouches…….. 38

3.3 *Tg(pax1b: eGFP)* enhancer trap fish line expressing eGFP in the developing pharyngeal pouches…… 40

3.4 Deficiency of *pax1a* and *pax1b* leads to defects in the development of ceratobranchial cartilage and reduced expression of *dlx2a* and *hand2*…… 42

3.5 Evaluation of apoptosis and cell proliferation rate in *pax1a* and *pax1b* deficiency embryos…… 46

3.6 Deficiency of *pax1a* and *pax1b* leads to defects in pharyngeal pouch morphogenesis and absence of endodermal expression of *fgf3, tbx1*

doi:10.6342/NTU202000783

and *edn1* in pharyngeal pouches……..…... 47

3.7 Pax1a and Pax1b regulate ceratobranchial cartilage formation by modulating expression of *fgf3*, *tbx1* and *edn1*…….…… 48

4. Dissusion…….…..... 52

5. Conclusion…….…..… 59

Reference……..…..… 60

Figures……. 67

Fig. 1. Embryonic expression level of *pax1a-201* and *pax1a-202*…. 67

Fig. 2. Developmental expression patterns of zebrafish *pax1a* gene. 68

Fig. 3. Developmental expression patterns of zebrafish *pax1b* gene. 70

Fig. 4. *pax1b* is expressed in pharyngeal pouches but not in the neural crest cells of pharyngeal arches…… 72

Fig. 5. Comparison of *pax1b* expression level between wild type and *Tg (pax1b: eGFP)* embryos.……..…….. 73

Fig. 6. Time lapse analyses of *Tg(pax1b:eGFP)* enhancer trap transgenic embryos reveals sequential segmental development of pharyngeal pouches…….…… 74

Fig. 7. Evaluation of specificity of *pax1a* MO and *pax1b* MO…..… 75

Fig. 8. Pax1a and Pax1b have redundant function in regulating pharyngeal cartilage development…… 77

Fig. 9. *pax1a*- and *pax1b*-deficient embryos generated by CRISPR-Cas9

doi:10.6342/NTU202000783

mutagenesis exhibit abnormality of hyoid cartilage and lack of ceratobranchial cartilages 1-4.…….…… 78

Fig. 10. Knockdown of *pax1a* and *pax1b* decreases expression of neural crest markers *dlx2a* or *hand2* or endodermal pouches marker *nkx2.3*……..... 80

Fig. 11. *pax1a*- and *pax1b*-deficient embryos display decrease or absence of *dlx2a* and *hand2* expression in pharyngeal arches. 81

Fig. 12. Reduced *dlx2a* expression in pharyngeal arches 3-4 in *pax1a*; *pax1b* morphants beginning at 22 hpf……..…… 82

Fig. 13. Similar levels of apoptosis and proliferation were observed in *pax1a*- and *pax1b*-deficient embryos…….…….. 83

Fig. 14. *pax1a*- and *pax1b*-deficient embryos exhibit morphogenetic defects and lack of *nkx2.3* or Alcama expression in the pharyngeal pouches……..… 85

Fig. 15. Reduced expressions of *edn1*, *fgf3*, or *tbx1* in pharyngeal pouches are detected in *pax1a*; *pax1b* morphant embryos..…. 86

Fig. 16. *pax1a*- and *pax1b*-deficient embryos exhibit absent *fgf3*, *tbx1* and *edn1* expression in pharyngeal pouches……..… 88

Fig. 17. Pax1b directly binds to PAX binding elements 5′ upstream of the *fgf3* gene..…… 89

Fig. 18. Western blot for Pax1 and Myc-Pax1 expression…...…….. 90

doi:10.6342/NTU202000783

Fig. 19. A proposed model describing the function of Pax1a and Pax1b in regulating pharyngeal pouch morphogenesis and ceratobranchial cartilage formation…… 91

Publication list……...…. 92

doi:10.6342/NTU202000783

1. Introduction

1.1 Craniofacial structure of zebrafish

The vertebrate head is an extremely complicated structure. The craniofacial structures are important for feeding, respiration and the production of endocrine hormones. Interruption of normal growth and differentiation of the craniofacial structure results in a variety of craniofacial abnormalities. Craniofacial syndromes include defects associated with craniosynostosis and clefts that interfere with physical and/or mental health. Craniofacial morphogenesis requires interactions among all three germ layers and coordinated three-dimensional movement. In zebrafish embryos, the craniofacial structure is composed of ventral pharyngeal arches, which is reiterated segments along the anterior- posterior axis, and a dorsal neurocranium. The pharyngeal arches are transient structures posterior to the eye and below the ear. The pharyngeal arches consist of cylinders of cranial neural crest cells (CNC) surrounding a core of mesoderm, lined externally by ectoderm and internally by pharyngeal endoderm. The ectoderm forms epidermis and sensory neurons; cranial neural crest cells give rise to cartilage and connective tissue; the paraxial mesoderm becomes muscles and endothelia cells; the endoderm forms pharyngeal pouches and contributes to thyroid, parathyroid and thymus (Knight and Schilling, 2006; Mork and Crump, 2015).

There are seven pairs of pharyngeal arches in zebrafish. Mandibular or Pharyngeal

doi:10.6342/NTU202000783

arch 1 (pa1) is composed of ventral Meckel's cartilages (m) to form the U-shaped lower jaw. Their posterior ends articulate with dorsally located Palatoquadrates (pq), which develop pterygoid processes that articulate with the ethmoid plate of neurocranium. Hyoid (pa2) consists of ventral large paired Ceratohyals (ch) and unpaired Basihyal (bh) cartilages in the midline. Ceratohyals articulate posteriorly with tiny Interhyals (ih) and the most dorsal, large and triangular Hyosymplectics (hs). Hyoid arch has grown posteriorly to form the Opercula(op) that eventually cover more posterior arches. Five posterior pharyngeal arches (pa3-pa7) or branchial arches (b1-b5) are composed of different paired ventrolateral Ceratobranchial (cb) cartilages 1-5 and Hypobranchial (hb) 1-4, and a ventral midline, basal component, Basibranchial (bb) cartilages 1-3 fused together and a separate bb 4. The first to fourth branchial arches support the gill arches, and the fifth branchial arches form teeth, three on each side at 5 days post fertilization (Schilling and Kimmel, 1997; Schilling et al., 1996).

The anterior neurocranium consists of two longitudinal rods of chondrocytes, the trabeculae cranii, that fuses across the midline to form the ethmoid plate. Polar cartilages lie at their posterior ends. Trabeculae fuse posteriorly with basicapsular commissures and parachordal cartilage underlying posterior regions of the brain. Lateral, anterior and posterior basicapsular commissures form in the neurocranium, the first two anterior and the last posterior to the auditory capsule. (Schilling and Kimmel,

doi:10.6342/NTU202000783

1997; Schilling et al., 1996).

1.2 Neural crest morphogenesis

All pharyngeal skeletons are derived from cranial neural crest cells. Neural crest cells characterized as a stem/progenitor cell population are unique to vertebrate embryos and are able to migrate extensively and differentiate into a variety of derivatives including sensory and autonomic ganglia, cartilage and bone of the face and pigment cells of the skin (Simoes-Costa and Bronner, 2015).

During gastrulation stage, neural crest cells are induced from ectodermal germ layer. When the neural plate closes to form the neural tube, the dorsal part of the neural fold expressing neural crest genes (*FoxD3* and *Sox10*), that reflect neural crest specification (Labosky and Kaestner, 1998; Southard-Smith et al., 1998). Neural crest cells initially reside in the neural plate border territory, where the lateral edges of the central nervous system. The neural plate border induction is regulated by the interaction of proneural gene activator FGFs signaling and inhibitors of WNT and BMP and Notch signaling (Streit et al., 2000). In response to these signaling module, several neural plate border specifier genes (*Tfap2a*, *Msx1*, *Zic1*, *Gbx2*, *Pax3/7*, *Dlx5/6*, *Gata2/3*, *foxi1/2* and *Hairy2*) are expressed (Khudyakov and Bronner-Fraser, 2009; Meulemans and Bronner-Fraser, 2004; Nichane et al., 2008). These transcription factors further conduct mutual cross-regulator interaction to stabilize their expression in the neural plate border and

doi:10.6342/NTU202000783

perform inhibitory interactions with neural transcription factor. As a result, a sharp boundary between the neural plate and the neural plate border is generated.

The neural plate border becomes segregated into medial premigratory neural crest and lateral preplacodal domains. The expression of key placodal regulators (*Six1*, *Eya1/2* and *Irx1*), which is induced by lateral neural plate border specifiers (*Foxi1/3*, *Gata2/3* and *Dlx5/6*), is established lateral to the neural crest domain (Grocott et al., 2012; Sato et al., 2010).

The first neural crest specifier genes expressed in the neural plate border are *FoxD3*, *Ets1* and *Snai1/2* in chick (Khudyakov and Bronner-Fraser, 2009). The neural plate border specifiers *Pax3/7* and *Msx1* regulate *FoxD3* expression (Simões-Costa et al., 2012). *Pax3/7*, *Msx1* and *Zic1* are conserved and crucial genes for the acquisition of neural crest identity directly activate a number of neural crest specifier genes in multiple species. A full suite of neural crest specifier genes (*Myb*, *Myc*, *prdm1a*, *FoxD3*, *Snai2*, *Ets1*, *Sox8/9/10* and *Pax3/7*) are then expressed to maintain neural crest identity.

Next, these neural crest specifiers activate the epithelial-to-mesenchymal transition (EMT) program, which allows delamination of the neural crest from the ectoderm and become a migratory cell type. The delamination of neural crests involves cell surface changes resulting in the dissociation of adherens junctons. A study in chick showed that a switch between type 1 cadherins (*Ecad* and *Ncad*) and type 2 cadherins (*Cad7* and

doi:10.6342/NTU202000783

Cad11) is required for neural crests delamination. FoxD3 also represses expression of *Ncad* and activates *Cad7* expression (Cheung et al., 2005; Dottori et al., 2001). Similarly Snail1/2 cooperates with Lmo4 to downregulate *Ncad* expression (Ferronha et al., 2013). Furthermore, Snail1/2 interacts with phosphorylated Sox9 to facilitate trunk neural crest delamination (Liu et al., 2013a). In addition, Snail2 represses another type 2 cadherin (Cad6b) which needs to be downregulated before neural crest delamination (Taneyhill et al., 2007).

Delamination and cell dispersion of epithelial-to-mesenchymal transition (EMT) are partially uncoupled in neural crest development. A study in *X. laevis* showed the dissociation of neural crest cells is mediated partly by Twist via repression of *Ecad* in the delaminating cells (Barriga et al., 2013). Another transcriptional repressor (Zeb2) identified in Chick plays similar role as Twist. Knockdown of Zeb2 maintains Ecad expression in migratory neural crest cells and results in aggregates of adherent neural crest cells in the vicinity of the neural tube (Rogers et al., 2013). Therefore, neural crest EMT is a two-step process. Neural crest cells first delaminate from the neural tube, a process involved in repression of *Cad6b* by Snail2 which allows neural crest cells to leave the neural tube, followed by cell dispersion which allows separation of neural crest into individual migratory cells, a process involved repression of *Ecad* by Twist and Zeb2.

doi:10.6342/NTU202000783

After delamination, migrating neural crest cells express various transcription factors for cell migration and for initiating differentiation. Neural crest specifier genes (such as *FoxD3, Est1* and *Sox8/9/10*), retained expression in some or all migratory cells, however, their expression in the migratory neural crest cells are regulated by different enhancer (Simões-Costa et al., 2012). In addition, they also positively self-regulated in order to continuously express in the migratory neural crest cells (Wahlbuhl et al., 2012).

In zebrafish, at 12 hpf (hours post fertilization), migratory cranial neural crest cells arise from dorsal and lateral region of neural ectoderm. CNC migrates in three streams at 15 hpf. The first (anterior-most) stream emanated from rhombomere (r) 1 and r2 enters the first (mandibular) pharyngeal arch (pa1), which gives rise to the jaw. The second (middle) stream emanated from r4 populates the second (hyoid) pharyngeal arch (pa2), which gives rise to the face. The third (posterior) stream emanated from r6, which progressively splits into two, three, four and eventually five cell groups, each separated by endodermal pouches of pharynx. The third stream populates the third and more caudal pharyngeal arches (pa3-7), which give rise to the components of the neck and the gills. These streams are separated by two cranial NC-free zones, which are located lateral to r3 and r5 (Yelick and Schilling, 2002). By larval stages, each pharyngeal arch contains specific cartilage derived from CNC and muscle derived from mesoderm core. The CNC skeletal derivatives are patterned through a combination of neural crest cell

doi:10.6342/NTU202000783

differences and adjacent tissue signals, including endoderm and ectoderm.

1.3 Pharyngeal anterior-posterior and dorsoventral patterning

Study in mouse indicates that nested expression of homeodomain factors, *Hox* genes, provides a combinatorial "Hox-code" to specify regional properties within anterior-posterior (AP) axis (Parker et al., 2016). Neural crest cells (NCCs) adjacent to rhombomere 2 (r2), which colonize PA1, do not express any *Hox* genes. Migrating NCCs from r4 into PA2 continues to express *Hoxa2* and *Hoxb3* but cease *Hoxb1* expression (Hunt et al., 1991; Hunter and Prince, 2002). By later stages (mouse E10.0) a pharyngeal NCC *Hox* code reveals nested gene expression. *Hoxa2* and *Hoxb2* expressed in PA2–4, *Hoxa3* in PA3–4 and *Hoxb3* and *Hoxd3* weakly in PA3 but strongly in PA4, and *Hoxd4* strongly expressed in PA4.

Hoxa2-null mice fail to correctly form PA2 skeletal derivatives, showing duplicated PA1-like structures (Gendron-Maguire et al., 1993; Minoux and Rijli, 2010). Conversely, ectopic expression of *Hoxa2* in PA1 suppresses the formation of PA1-derived jaw structures, and results in duplication of PA2 derivatives (Kitazawa et al., 2015). The evolutionarily conserved function of *Hoxa2* gene in craniofacial morphogenesis was identified across jawed vertebrates, such as in chick, *Xenopus* and zebrafish (Grammatopoulos et al., 2000; Pasqualetti et al., 2000).

Studies in zebrafish indicate that skeletal precursors of dorsoventral (DV) axis are

doi:10.6342/NTU202000783

determined by complex interactions between multiple signaling pathways, in particular Endothelin-1 (Edn1), Bone Morphogenetic Protein (BMP), and Jagged–Notch signaling. These signals appear to act through several families of transcription factors, including Dlx, Msx, and Hand, to establish dynamic zones of skeletal differentiation. The diversification of the vertebrate facial skeleton, including the evolution of the jaw, was driven largely by modifications downstream of a conversed pharyngeal DV patterning program (Medeiros and Crump, 2012).

1.4 Requirement of endoderm for craniofacial cartilage formation

A previous study showed that pharyngeal endoderm is important in cartilage development and patterning of the CNC-derived pharyngeal skeleton. The pharyngeal pouches are segmental series of epithelial structures derived from pharyngeal endoderm. In vertebrate, the formation of endoderm and mesoderm is specified by Nodal signaling (Schier and Shen, 2000). sox32/Casanova (*cas*), which is a transcription factor downstream of Nodal signaling is essential for endoderm development (Alexander et al., 1999). The zebrafish *cas* mutants lacked all pharyngeal arch cartilages and absence of trabeculae by Alcian Blue staining at 4-5 days. Formation of three streams of *dlx2a*-labeled CNCs was initially identified in *cas* mutants at 23s stage. However, three streams of *dlx2a*-positive neural crest cells progressively lost from stream III to stream I in *cas* mutants during 24 to 48 hpf. Transplantation results further demonstrated that the

doi:10.6342/NTU202000783

sox-related transcription factor, *cas*, is required non-autonomously to maintain the identify and survival of pharyngeal arch cartilages (David et al., 2002).

Characterization of zebrafish mutants further demonstrates the involvement of several genes in the pharyngeal pouch development. Tbx1 is a member of T-box transcription factor family. *tbx1* is expressed in the primordia of the pharyngeal arches (pa1 to pa7) at 20s stage and is localized to the arch epithelium and mesodermal core of pharyngeal arches by 27 hpf (Piotrowski et al., 2003). At 30 hpf, *tbx1* is detected in the endodermal pouches and arch muscles, between 24 hpf and 72 hpf *tbx1* was expressed in the cardiac region, pharyngeal arch and otic vesicle in zebrafish. Retinoid acid (RA) signaling is essential for patterning the endoderm of the posterior pharyngeal arches. The defects produced by a loss of Tbx1 highly resemble those induced by hyper- and hypo- RA. Treat different dose RA could produce an altered *tbx1* expression pattern. Repression of *tbx1* expression was most evident at 36 hpf, 24 hours after RA treatment at 12.5 hpf for 1.5 hours. In addition, RA could repress *tbx1* expression in a dose-dependant manner (Zhang et al., 2006). Embryos of *tbx1*/*van gogh* (*vgo*) mutants revealed defects in the ear, thymus, and pharyngeal arches. Alcian Blue staining revealed drastically reduced mandibular and hyoid arches, and the absence of five branchial arches in *vgo/tbx1* mutants. Tbx1 is shown to be required non-autonomously in neural crest derived pharyngeal structures. Results of *in situ* hybridization and rescue

doi:10.6342/NTU202000783

experiments demonstrated that *vgo/tbx1* regulates *edn1* expression and Edn1 further control expression of *hand2*, a bHLH transcription factor expressed in the neural crest cells (Piotrowski et al., 2003). Function of Tbx1 in pharyngeal pouch morphogenesis was later characterized in *vgo/tbx1* mutant, revealing failure in the initiation of pouch outpocketing (Choe and Crump, 2014). *vgo/tbx1* mutant also retained expression of the immunoglobulin-domain protein Alcama, a marker of maturing pouches, despite the absence of morphological pouches. Transgenic rescue experiments by stably integration of *nkx2.5*: Tbx1 versus *nkx2.3*: Tbx1 transgenes indicate that mesodermal Tbx1 is adequate for pouch morphogenesis but not later cartilage formation. A two-step model describing Tbx1 function in pouch morphogenesis was then proposed. Tbx1 promotes expression of *wnt11r* and *fgf8a* in different domains of the mesoderm where Wnt11r initiates pouch morphogenesis via epithelial destabilization and Fgf8a directs following pouch outgrowth. Loss of *wnt11r* and *fgf8a* phenocopies *vgo/tbx1* mutant phenotype (Choe and Crump, 2014).

sucker (suc)/endothelin 1 (edn1) encodes a 21-amino-acid secreted ligand and is expressed in central mesenchymal cores of arch paraxial mesoderm, ventral epithelia of surface ectoderm and pharyngeal endodermal pouches (Miller et al., 2000). Within the pharyngeal pouches, expression is restricted to posterior, ventral epithelia. In *suc/edn1* mutant embryos, ventral cartilages of mandibular and hyoid arches such as Meckel's

doi:10.6342/NTU202000783

cartilage and ceratohyal are reduced and fused to the dorsal cartilages of the same arches. Before chondrogenesis, *suc/edn1* mutant embryos have severe defects in expression of *hand2, dlx2a, msx1a, msx1b, gsc, dlx3b* and *epha3* in the ventral arch neural crest cells. The role of Edn1 in the formation of ventral cartilages and joints in the anterior pharyngeal arches is further analyzed (Miller et al., 2003). Ventral pharyngeal specification involves repression of dorsal and intermediate (joint region) fates. Two Edn1 downstream target genes, *bapx1/nkx3.2* and hand2, specify joints and ventral pharyngeal fates. Additionally, Edn1 can bind to Ednrb receptor expressed in pharyngeal pouches to stabilize Alcama protein. Alcama then binds to Nadl1.1 expressed in neural crest cells to regulate expression of *hand2, dlx3b, dlx5a, dlx6a* which are essential for neural crest differentiation (Choudhry et al., 2011). Edn1 binds to one or both of the two known mammalian G protein-coupled endothelin receptor, Ednra (endothelin type A receptor) and Ednrb. There are two zebrafish ednra genes, *ednraa (ednra2)* and *ednrab (ednra1). ednrab* is expressed in the migrating and postmigratory neural crest cells of the pharyngeal arches and ectodermal epithelium while *ednraa* is identified in postmigratory neural crest cells within arches at 24 hpf. Combined loss of Ednraa and Ednrab eliminates the lower jaw similar to *suc/edn1* mutants (Nair et al., 2007). *ednrb1* expression in the endoderm is compatible with our hypothesis that Edn1 signals to the endoderm to regulate Alcama levels (Choudhry et

doi:10.6342/NTU202000783

al., 2011).

Embryos treated with SU5402 inhibitor to prevent Fgf signaling failed to develop any viscerocranial cartilage and form severely reduced neurocranium at 96 hpf (David et al., 2002). *fgf3* expression is detected in the mid-hindbrain boundary, rhombomere 4 and in pharyngeal endoderm region beneath rhomboneres 1-3 at 12s stage. Endodermal expression of *fgf3* is restricted to three formed endoderm pouches at 25s stage. At 24 hpf, *fgf3* expression in the anterior pharyngeal pouches decreases but is maintained in two posterior pharyngeal pouches. *fgf3* morphants displayed hyoid arch with inverted AP polarity and loss of branchial arches except the 7th arch. Down regulation of *dlx2a* expression in stream III cranial neural crest cells was identified in *fgf3* morphant at 24 hpf, indicating that in *fgf3* is required for posterior cranial neural crest cells to maintain *dlx*2a expression (David et al., 2002; Walshe and Mason, 2003a). *fgf8* started to be expressed in the first pouch endoderm and endoderm associated with posterior arches at 16 hpf. Both *fgf8* and *fgf3* are expressed by endoderm associated with the developing jaw such as first endodermal pouch at 30 hpf. *fgf8* mutant phenotype in pharyngeal pouches and cartilages is relatively mild, suggesting other Fgfs such as Fgf3 functions redundantly in patterning pharyngeal arches. Although *fgf8* mutnats and *fgf3* morphants had largely normal pouches, *fgf8* mutant; *fgf3* morphant embryos did not develop pouches and had severe reductions in size of mandibular cartilages and absence of hyoid

doi:10.6342/NTU202000783

cartilages and posterior branchial cartilages. Therefore, Fgf signaling in the mesoderm and segmented hindbrain controls the segmentation of the pharyngeal endoderm into pouches; this is essential for the subsequent patterning of pharyngeal cartilages (Crump et al., 2004a; Walshe and Mason, 2003b).

integrinα5 (itga5) is expressed in pharyngeal endoderm with a pattern that spatially and temporally corresponding to regions of pouch formation and cranial neural crest cells. Expression of *itga5* is found in cranial neural crest, otic placode and pharyngeal endoderm at 5s stage. Strong *itga5* expression throughout pharyngeal endoderm, including the first pouch is identified at 18 hpf. By 26 hpf, expression of *itga5* is found in the fourth pouch whereas *itga5* is no longer expressed in the first pouch. At 38 hpf, strong *itga5* expression is identified in the sixth pouch while *itga5* is not expressed in the fourth pouch. Expression of *itga5* is also detected in patchy zones of pharyngeal crests. Specific defects in the formation of the first pouch and loss of the anterior Hyomandibula (ahm)and Symplectic (sy) cartilages of hyoid cartilages was identified in *itga5* mutant larvae; this phenotype is attributed to lack of pouch-derived signals from the first pouch to promote the growth and survival of neural crest cells in the adjacent ahm and sy of hyoid cartilage (Crump et al., 2004b). Itga5 was also implicated in posterior pharyngeal arch development. Prdm1a was shown to be required for posterior ceratobrachial cartilage development. Overlapping expression of *prdm1a* and *itga5* was

doi:10.6342/NTU202000783

identified in the posterior arches and decreased *itga5* expression was detected in *prdm1a* mutants, indicating *prdm1a* acts upstream of *itga5*. Loss of *dlx2a* expression in the ceratobranchial cartilage 2-5, and cell proliferation in *prdm1a* mutants can be rescued with *itga5* mRNA injection. Therefore, Prdm1a and Itga5 are both required for posterior pharyngeal arch development (LaMonica et al., 2015).

1.5 Pax1

Vertebrate Paired-box containing transcription factor *Pax* genes were identified based on their homology in DNA-binding motif with the *Drosophila melanogaster paired* gene. Pax transcription factor family members contain two DNA-binding domains (the paired domain and the homeodomain), a co-factor-interacting domain (the octapeptide) and C-terminal activation and repression domains. In mammals, nine Pax members are grouped into four subfamilies such as Pax1/9, Pax2/5/8, Pax3/7, and Pax4/6, according to their structural similarity and the sequence homology (Underhill, 2000). All Pax proteins contain paired domain and transactivation domain. Pax1/9 members contain no homeodomain but contain octapeptide which is highly conserved eight-amino acid [(H/Y)S(I/V)(N/S)G(I/L)LG] domain as protein-protein interaction motif. Pax2/5/8 members contain partial homeodomain and octapeptide. Homeodomain is helix-turn-helix DNA-binding motif. Pax3/7 members contain full homeodomain and

doi:10.6342/NTU202000783

octapeptide; Pax4/6 members contain full homeodomain but no octapeptide. *Pax* gene family are important regulatory genes and are essential for cell lineage specification and the development of a variety of organs and tissues. Mutation in human *Pax3* gene results in Waardenburg syndrome while human *Pax6* mutation causes Aniridia. Mutation in human *Pax2* or *Pax8* gene leads to Renal coloboma or congenital Hypothyroidism while human *Pax9* mutation causes Oligodontia (Underhill, 2000). Several *Pax* genes are required for the differentiation of various neural crest derivatives. For examples, *Pax3* and *Pax7* regulate proliferation of craniofacial neural crest cells, *Pax9* controls tooth and craniofacial skeleton development while *Pax1* and *Pax9* are essential for thymus, thyroid and parathyroid development. (Monsoro-Burq, 2015).

Human *PAX1* is essential for the development of vertebral column. Patients with Klippel-Feil syndrome was identified by shortness of the neck and cervical vertebrae fusion due to alteration of*PAX1* sequence such as missense, silent, intronic changes or a silent change within the paired box (McGaughran et al., 2003). While *PAX1* homozygous variant G166V within paired box is identified in the autosomal recessively inherited OFCS (otofaciocervical syndrome) disorder characterized by facial dysmorphism, external ear anomalies, branchial cysts, anomalies of vertebrae and the shoulder girdle, and mild intellectual disability (Pohl et al., 2013).

In mouse embryos, *Pax1* is expressed in the developing sclerotomes and later in

doi:10.6342/NTU202000783

the anlagen of intervertebral discs along whole vertebral column. Mice *undulated (un)* homozygous mice containing a Gly-Ser replacement in the paired box of *Pax1* exhibit vertebral abnormalities along the entire anterior-posterior axis (Balling et al., 1988). A *Pax1* null mutant *(Un^s)* was created by gene targeting and homozygous *Pax1* null mice showed similar phenotype as natural *undulated* mutant mice. Analysis of heterozygous *Pax1* knockout *(Un^s)* mice further demonstrated that *Pax1* is haploinsufficient in the development of some skeletal elements of vertebral column and sternum (Wilm et al., 1998). *Pax1* is also transiently expressed in the developing limb buds that are important for the development of pectoral girdle demonstrated by different alleles of *undulated* mutants (Timmons et al., 1994). *Pax1* was also shown to be required for the chondrogenic differentiation of sclerotomal cells by transactivating *Bapx1/Nkx3.2* gene expression in the sclerotome. *Pax1*;*Pax9* double mutant mice lack *Bapx1* expression in the sclerotome, indicating *Bapx1* is a direct target of Pax1 and Pax9 (Rodrigo et al., 2003). A study using *Pax1*;*Pax9* double mutant mice further demonstrated functional redundancy between *Pax1* and *Pax9* during vertebral column development and their roles in the control of cell proliferation during early sclerotome development (Peters et al., 1999). *Pax1* is also expressed in the embryonic thymus and expression of *Pax1* protein can be identified in the epithelium of the third pharyngeal pouch which produce part of the thymus epithelium. *Pax1* expression continues during thymus development

doi:10.6342/NTU202000783

and *Pax1* expression in thymus epithelium is essential to form the thymus microenvironment which is required for normal T cell maturation (Wallin et al., 1996).

Chick *Pax1* is detected in the sclerotome, limbs and shoulder girdle, (Takimoto et al., 2013). Although mouse Pax1 was implicated in promoting chornodrogenic differentiation of sclerotomal cells through induction of *Bapx1/Nkx3.2* expressed, chick Pax1 was identified to inhibit chondrocyte maturation, independently of *Bapx1/Nkx3.2*. Forced expression of *Pax1* in chick forelimb produced shortened skeletal elements with reduction of proteoglycan accumulation in cartilage. Overexpression of *Pax1* in cultured chondrocytes lacked accumulation of cartilaginous proteoglycan which is accompanied by downregulation of *Sox9*, *Col2a1*, *Chm1* and *Agc1*. These results indicate that chick Pax1 acts as a negative regulator of chondrocyte maturation via antagoning Sox9 expression (Takimoto et al., 2013). Similar expression of *pax1* in the sclerotome and in the pharyngeal pouch was identified in *Xenopus* embryos (Sanchez and Sanchez, 2013).

In medaka fish, similar expression of *pax1* and *pax9* was observed in the pharyngeal pouches and sclerotome. Unlike the mouse, both medaka *pax1* and *pax9* are indispensable for the development of the vertebral body and neural arch; knockdown of *pax1* showed absence of some vertebral arches and scoliosis (Mise et al., 2008). However, *pax1* plays crucial roles in pouch segmentation in medaka embryos. TALEN-generated *pax1* mutants did not form pharyngeal pouches posterior to the second arch.

doi:10.6342/NTU202000783

pax1 mutant exhibited complete loss of the ceratobranchial cartilage 1-4, deformed basibranchial cartilage of pharyngeal arches 3-6, projection of cranial nerves IX and X were specifically suppressed and loss of thymus-specific expression of *foxN1* (Okada et al., 2016).

Zebrafish genome has two *pax1* paralogues, *pax1a* and *pax1b*, which respectively locates on chromosome 17 and 20 and presents different exon-intron structure. *pax1a* and *pax1b* shares 70.4% nucleotide sequence and 77.6% amino acid sequence identity in the coding region as well as 97.9% amino acid sequence identity in the paired domain. A previous publication showed that *pax1b* is expressed in the endodermal pharyngeal pouches, caudal somites, notochord, and pectoral fin bud. Morpholino knockdown of *pax1b* revealed defects in the vertebral column, tail, pharyngeal skeleton, and pectoral fin (Liu et al., 2013b).

1.6 The specific aims of this thesis

1. Investigation of pharyngeal pouch morphogenesis by time-lapse imaging of *Tg(pax1b:eGFP)* transgenic zebrafish which expressing eGFP in the pharyngeal pouches.
2. Investigation of overlapping or distinct function of zebrafish *pax1a* and *pax1b* in pharyngeal pouch morphogenesis and subsequent pharyngeal cartilage development. To achieve this goal, we performed following experiments.

doi:10.6342/NTU202000783

A. Examination of developmental expression pattern of *pax1a* and *pax1b*.

B. Investigation of function of *pax1a* and *pax1b* by morpholino-mediated knockdown and CRISPR-Cas9 mutagenesis.

C. Examination of downsteam affected genes located in pharyngeal pouches or neural crest cells of pharyngeal arches in control and *pax1a*- and/or *pax1b*-defient embryos.

D. Confirmation of downstream target genes of *pax1a* and *pax1b* by chromatin immunoprecipitation.

doi:10.6342/NTU202000783

2. Materials and methods

2.1 Zebrafish strains and husbandry

Adult zebrafish, including ASAB wild type, *pax1a*^{as36} mutant, *pax1b*^{as37} mutant and *Tg(pax1b:eGFP)*^{as38Et} transgenic fish were reared in a high-density, self-circulating aquaculture system (Aqua blue) or a 20-L aquarium equipped with a filtration and aeration apparatus under a photoperiod of 14 h light and 10 h dark. Embryos were kept at 28.5℃ and morphological criteria were defined as described (Kimmel et al., 1995). All animal procedures were approved by the Academia Sinica Institutional Animal Care & Use Committee (Protocol ID: 15-12-918).

2.2 Generation of *Tg(pax1b:eGFP)* enhancer trap transgenic fish

A Tol2 transposon containing SAGVG (splice acceptor-Gal4-VP16;UAS:eGFP) plasmid DNA and Tol2 transposase RNA were co-injected into 1–2 cell ASAB zygotes (Davison et al., 2007; Kawakami et al., 2004; Urasaki et al., 2006). Injected F0 embryos were reared to adulthood, and F1 embryos were then produced by outcrossing with wild type. The F1 embryos with eGFP expression in the pharyngeal arch region, as detected by fluorescence microscopy, were raised to adulthood. NlaIII or DpnII linker-mediated PCR was conducted to identify the insertion site of SAGVG plasmid, as described (Davison et al., 2007). In the *Tg(pax1b:eGFP)* enhancer trap transgenic fish, it was determined that the SAGVG plasmid had been inserted 3´ downstream of the *pax1b*

doi:10.6342/NTU202000783

gene (between 48,693,260 and 48,692,881) in chromosome 20.

2.3 Generation of *pax1a* mutants and *pax1b* mutants via CRISPR-Cas9 genome editing system and off-target analysis

pax1a mutants and *pax1b* mutants were produced using a CRISPR-Cas9 system. ZiFiT Targeter software was used to design three sgRNAs each targeting exon 2 of the *pax1a* and *pax1b* genes. Complementary oligomers of individual sgRNAs were aligned and cloned into BsmBI-digested pT7-gRNA vector (Jao et al., 2013). Individual sgRNAs were synthesized using BamHI-linearized pT7-gRNA and the MEGAshortscript T7 transcription kit (Invitrogen). Mixtures of 100 pg *pax1a* sgRNA or *pax1b* sgRNA and 250 pg Cas9 protein (Tools) were incubated at room temperature (RT) for 5 min before injection into 1-cell zygotes. Genomic DNA was isolated from pools of 10 injected embryos at 30 hpf. PCR for *pax1a* was performed using forward (5’- TAT TTT CCA TTG CCT AAG TTG A-3’) and reverse (5’- TAT TGC TGA CCG TAT GGG CTG AA-3’) primers, while PCR for *pax1b* was conducted using forward (5’- GCG CGG CTT CAG TGA CAG ATT TTA-3’) and reverse (5’- AGT TTG GAG CCG GTG GGT GAC A-3’) primers. Amplified DNA was digested with T7 endonuclease I (T7E1) to evaluate insertion and deletion (indel) efficiency. Embryos injected with the sgRNA displaying the highest indel efficiency were reared to adulthood. Genomic DNA isolated from clipped tail fin of adult F1 fish was subjected to

doi:10.6342/NTU202000783

high resolution melting (HRM) analyses to screen for suitable indels within exon 2 of *pax1a* or *pax1b* gene using forward (5'- TAT TTT CCA TTG CCT AAG TTG A-3') and reverse (5'- TGG ACC CTG TTT CGT TGT ATC-3') or forward (5'- GCG CGG CTT CAG TGA CAG ATT TTA-3') and reverse (5'- GGG AAG CGG CCG ACC ATT GAC-3') primers.

Four off-target genes including *pax1b* (2 mismatches), *pax2b* (2 mismatches), *pax5* (3 mismatches) and *pax9* (2 mismatches) were predicted for *pax1a* sgRNA and three off-target genes such as pax1a (2 mismatches), pax5 (3 mismatches) and *pax9* (3 mismatches) were predicted for *pax1b* sgRNA by ZiFIT program. To analyze whether indel occurs in these off-target genes, PCR and DNA sequencing was conducted using genomic DNA isolated from clipped tail fin of 39 $pax1a^{as36}$ and 27 $pax1b^{as37}$ F1 adults and respective primer pair spanning predicted off-target region of individual off-target genes. Primer pair (forward: 5'- ATT CGT CTG CGT TTG TTT ATT C-3'and reverse: 5'- TGC GCG AGC TCC ACG ATT CT-3') was used for *pax2b*. Primer pair (forward: 5'- CAG CTG GGG TGA ACA TAA CG-3' and reverse: 5'- CGC CCA TTT ACA AAC ACC CC-3') was used for *pax5* while primer pair (forward: 5'- ACG TGC CTA AGT TAC CGA ATG T-3'and reverse: 5'- AAC TGG GCC AAC TCT ACT ATC CT-3') was used for *pax9*. $pax1a^{as36}$ and $pax1b^{as37}$ F1 adults without off-target editing were then maintained. Primer pairs used to evaluate *pax1a* or *pax1b* predicted off-target regions

doi:10.6342/NTU202000783

were the same as those used for previous HRM analysis.

These genes in *pax1a*^{as36} and *pax1b*^{as37} mutants are found no indel occurred. However, we did identify 24-bp deletion of *pax2b* which resulted deletion of 8 amino acids in half of *pax1a*^{as36} mutants. We then maintained *pax1a*^{as36} mutants without *pax2b* edition for subsequent experiments.

pax1a$^{-/-}$ and *pax1b*$^{-/-}$ homozygous mutants were viable, and F4 homozygous adults were maintained. To obtain a higher frequency (1/4) of *pax1a*$^{-/-}$; *pax1b*$^{-/-}$ double mutant embryos, the *pax1a*$^{-/-}$ mutant was first crossed with the *pax1b*$^{-/-}$ mutant to generate *pax1a*$^{+/-}$; *pax1b*$^{+/-}$ mutants. The *pax1a*$^{+/-}$; *pax1b*$^{-/-}$ mutant and the *pax1a*$^{-/-}$; *pax1b*$^{+/-}$ mutant adults were then identified by sequencing progeny from incrossed adult *pax1a*$^{+/-}$; *pax1b*$^{+/-}$ mutants. Adult female and male *pax1a*$^{+/-}$; *pax1b*$^{-/-}$ mutants and the *pax1a*$^{-/-}$; *pax1b*$^{+/-}$ mutants were maintained. *pax1a*$^{-/-}$; *pax1b*$^{-/-}$ double mutant embryos were then generated by incrossing either the *pax1a*$^{+/-}$; *pax1b*$^{-/-}$ mutant adults or the *pax1a*$^{-/-}$; *pax1b*$^{+/-}$ mutant adults.

2.4 Morpholino-mediated knockdown

Translation-blocking morpholino oligonucleotides (MOs) and respective controls with five mismatched bases (5mm) were designed by Gene Tools for *pax1a* and *pax1b*. The sequence of the *pax1a* MO, which consists of 13 bases in the 5′ untranslated region and 12 bases in the coding region, is 5’-TGT TTG CTC CAT TTG CTT TTG CGA T-3’

doi:10.6342/NTU202000783

(start codon is underlined). The corresponding 5mm *pax1a* MO sequence is 5'-TGT *ATC* CTC *GAT* TT*C* CTT TT*C* CGA T-3' (start codon is underlined and 5 mismatched bases are italicized). The sequence of *pax1b* MO, which is comprised of 21 bases in the 5′ untranslated region and 4 bases in the coding region, is 5' - GCA TTG TGA TAT TTC CCT ATA CAG C-3' (start codon is underlined). The corresponding 5mm *pax1b* MO sequence is 5'- GCA TT*C* T*C*A TAT TT*G* CCT ATA *GAC* C-3' (start codon is underlined and 5 mismatched bases are italicized). Individual MOs were diluted with Danieau buffer, followed by injection of *pax1a* MO (0.75, 1.5 or 5 ng), *pax1b* MO (1.5, 5 or 10 ng), *pax1a* MO and *pax1b* MO (0.75 ng each) or 5mm *pax1a* MO and 5mm *pax1b* MO (0.75 ng each) into 1-2 cell zygotes using a Nanoject II automatic injector (Drummond).

2.5 Construction of *pax1a*-eGFP and *pax1b*-eGFP for testing MO knockdown specificity

Respective 318 bp or 267 bp DNA segment containing MO targeting sites of *pax1a* or *pax1b*, were cloned into a pcDNA3-eGFP vector. To generate *pax1a*-EGFP construct, primer pair 5'-**GAA TTC GAA TTC** TGA AGG GAC ACT TTA ACA TAG ACG-3 and 5'-**ACC GGT ACC GGT** TCA CTT TGT TTG TAG TCC CGT ATG-3' (EcoR1 and Age1 are indicated as boldface) was used. To generate *pax1b*-EGFP construct, primer pair 5'-**GAA TTC GAA TTC** TGC ACG GGA CCA CAG CAG CAC-3' and

doi:10.6342/NTU202000783

5’-**ACC GGT ACC GGT** GAG CCG GTC TCG TTG TAT CTG G-3’ (EcoR1 and Age1 are indicated as boldface) was used. To analyze the specificity of *pax1a* MO and *pax1b* MO, *pax1a*-EGFP or *pax1b*-EGFP plasmid (20 pg) together with 0.75 ng *pax1a* MO or *pax1b* MO were microinjected into 1 cell zygotes. 1 cell zygotes injected with *pax1a*-EGFP or *pax1b*-EGFP plasmid together with 5mm *pax1a* MO or 5mm *pax1b* MO were used as control.

2.6 mRNA synthesis, i*n situ* hybridization, immunofluorescence and TUNEL assay

To synthesize various antisense RNAs for *in situ* hybridization, plasmid DNA was linearized by restriction enzyme and RNA was produced using DIG or fluorescein RNA labeling kit (Roche) and SP6 (Roche) or T7 (Invitrogen) RNA polymerase. RNA probes were generated as follows (restriction sites and promoters in parentheses): *dlx2a* (BamHI, T7), *edn1*(NcoI, SP6), *fgf3* (NcoI, SP6), *hand2* (NcoI, SP6), *nkx2.3* (NcoI, SP6), *nkx2.7* (NcoI, SP6), *pax1a* (NcoI, SP6), *pax1b* (NotI, T7) or *tbx1* (NotI, T7).

In situ hybridization for whole-mount embryos was performed as described (Thisse and Thisse, 2008). To perform immunofluorescence with the zn-5 antibody, 24 and 36 hpf embryos were fixed in 4% paraformaldehyde at room temperature (RT) for 1 h, followed by fixation at 4℃ overnight. After PBST washes, embryos were dehydrated with PBST/methanol series and stored in methanol at -20℃. After passing through a rehydration series, embryos were incubated with collagenase (type IV, final

doi:10.6342/NTU202000783

concentration of 1 μg/μl, Sigma) at RT for 18 min and then washed with PTD buffer (1x PBS, 1% DMSO, 0.3% TritonX-100) twice. Embryos were then fixed in 4% paraformaldehyde for 20 min and washed with PTD buffer. After blocking with 0.5x blocking solution in PBST at RT for 1 h, embryos were incubated with zn-5 antibody (ZIRC, 1:100) diluted in 0.5x blocking solution in PBST at 4℃ overnight. After PBST washes, embryos were incubated with anti-mouse Alexa Fluor 488 (1:200) diluted in 0.5x blocking solution in PBST at 28℃ for 1 h and were later washed with PBST. Embryos were incubated with Hoechst 33342 (1:1000, Life Technologies) diluted in PBST for 1 h and washed with PBST.

To conduct double fluorescence *in situ* hybridization, pre-hybridized embryos were incubated with hybridization buffer containing fluorescein-labeled RNA probe at 65℃ overnight. After several buffer (50% formamide, 5x SSC, 0.1% tween 20, pH 5.0) washes, embryos were pre-hybridized with hybridization buffer for 2 h, followed by incubation with hybridization buffer containing digoxigenin-labeled RNA probe at 65℃ overnight. After washing with SSC buffer to remove excess RNA probes, embryos were incubated with 1x blocking solution at RT for 1 h, followed by incubation of anti-digoxigenin-POD antibody (1:1000) diluted in 0.5x blocking solution at 4℃ overnight. Embryos were then washed several times with PBST and incubated with TSA-Cyc 3 (1:50, Perkin Elmer) diluted in Plus Amplification Diluent at 28℃ for 1 h. Embryos

doi:10.6342/NTU202000783

were then washed with PBST, dehydrated with a methanol series and incubated with 1% H_2O_2 in methanol at RT for 30 min. After rehydration, embryos were blocked in 1x blocking solution at RT for 1 h, followed by incubation with anti-fluorescein-POD antibody (1:1000) diluted in 0.5x blocking solution at 4℃ overnight. After several PBST washes, embryos were incubated with TSA- fluorescein (1:50) diluted in Plus Amplification Diluent at 28℃ for 1 h, followed by PBST washes.

To perform fluorescence whole-mount *in situ* hybridization for *dlx2a* and immunofluorescence for PCNA, 26 hpf embryos that had been fixed with 4% paraformaldehyde were treated with proteinase K (10 μg/ml) at 28℃ for 12 min and later hybridized with digoxigenin-labeled *dlx2a* at 65℃ overnight. After RNA probe washes, embryos were blocked in 2x blocking solution in PBST at RT for 1 h before incubation with anti-digoxigenin-POD (1:1000, Roche) diluted in 1x blocking solution in PBST at 4℃ overnight. After several 15 min PBST washes and a rinse with Plus Amplification Diluent, embryos were then incubated with TSA-fluorescein (1:50) in Plus Amplification Diluent at 28℃ for 1 h and later washed with PBST for 10 min two times. After blocking with 0.5x blocking solution in PBST, embryos were incubated with mouse monoclonal anti-PCNA antibody (PC10, 1:200, Abcam) diluted with 0.5x blocking solution in PBST at 4℃ overnight. After PBST washes, embryos were incubated with anti-mouse Alexa Fluor 568 (1:200, Invitrogen) at 28℃ for 1-3 h and

doi:10.6342/NTU202000783

washed with PBST. Embryos were then incubated with Hoechst 33342 (1:1000) diluted in PBST for 1 h and washed with PBST.

To perform fluorescence whole-mount *in situ* hybridization for *dlx2a* in combination with the TUNEL assay, fixed embryos were subjected to *in situ* hybridization using digoxigenin-labeled *dlx2a* or *pax1a* as described above. Apoptotic cells were then labeled based on manufacturer's protocol using an *In situ* cell death detection kit, TMR red (Roche). Finally, labeled embryos were incubated with Hoechst 33342 (1:1000) diluted in PBST for 1 h and washed with PBST.

2.7 Alcian blue staining

96 hpf embryos were fixed in 4% paraformaldehyde at 4℃ overnight. After several PBS washes, embryos were rinsed with acid alcohol (70% ethanol and 0.37% HCl). Embryos were then stained with 0.1% Alcian Blue 8GX in acid alcohol for 4 h at RT and destained in acid alcohol overnight. After rehydration in PBS, embryos were digested with 1% trypsin for 1 h at 37℃. Embryos were then washed with PBS several times and stored in 70% glycerol.

2.8 Chromatin immunoprecipitation

Embryos (32-36 hpf) that had been injected with 30 pg *pax1b-Myc* plasmid DNA were dechorionated with pronase (P6911, Sigma). One hundred injected-embryos were washed with 1x PBS containing 2x PI (Protease Inhibitor Cocktail tablet, diluted from

doi:10.6342/NTU202000783

50x, Roche) and 2 mM PMSF (Phenylmethanesulfonyl fluoride, P7626, Sigma), before being fixed with 37% formaldehyde (final concentration of 1%) diluted in 1x PBS containing 2x PI and 2 mM PMSF for 15 min at RT. The embryos were then incubated with glycine (final concentration 125 mM) for 10 min, and washed three times with ice-cold 1x PBS containing 2x PI and 2 mM PMSF. Embryos were lysed by pipetting up and down in 600 μl ice-cold cell lysis buffer (10 mM Tris-HCl, pH 8.0, 10 mM NaCl, 0.5% NP-40, 2x PI and 2 mM PMSF) on ice for 15 min. After centrifugation, the nuclear pellet was resuspended in 600 μl nuclei lysis buffer (50 mM Tris-HCl, pH 8.0, 10 mM EDTA, 1% SDS, 2x PI and 2 mM PMSF), and then placed on ice for 20 min. Nuclei extract was aliquoted (200 μl) into a 1.5 ml Eppendorf tube and sonicated with a Bioruptor Pico sonicator (Diagenode) at the following settings: 30 sec ON and 30 sec OFF for 5 cycles for 5 times. The nuclei extract was spun down every 5 cycles and cooled on ice every 10 cycles. After sonication, 5 μl nuclei extract was used to verify that the length of DNA fragments was mostly between 200-600 bp. The sonicated nuclei extracts were then centrifuged at 14,000 rpm for 15 min at 4℃ to remove debris. The supernatants were pooled and stored at -80℃ for up to 3 months.

Before antibody incubation, the chromatin/DNA extract was pre-cleaned with Dynabeads ® Protein G (Invitrogen). Fifty microliters of 50% Dynabeads ® Protein G slurry was transferred to a 1.5 ml tube and washed three times with 1 ml of 1%

doi:10.6342/NTU202000783

BSA/PBS. The chromatin/DNA extract was incubated with washed Dynabeads ® Protein G for 1 h at 4℃. The pre-cleaned chromatin/DNA extract was diluted 10-fold with IP dilution Buffer (50 mM Tris-HCl, pH 8.0, 150 mM NaCl, 2 mM EDTA, 1% NP-40, 0.1% SDS, 2xPI, 2mM PMSF). One percent of the diluted chromatin/DNA extract was saved as the input control and stored at -80℃. The remainder of diluted chromatin/DNA extract was divided into two parts for incubation with either mouse anti-Myc antibody (Cell Signaling) or mouse IgG antibdoy. Five micrograms of antibody (IgG or anti-Myc) was added to the diluted chromatin/DNA extract and the mixture was rotated at 4℃ overnight. Fifty microliter of 50% Dynabeads ® Protein G slurry was transferred to a 1.5 ml tube and washed three times with 1 ml of PBS containing 1% BSA, 2x PI and 2 mM PMSF. After washing, Dynabeads ® Protein G were blocked with 1 ml of blocking solution (1% BSA, PBS, 2x PI, 2 mM PMSF), rotating at 4℃ overnight. After removing blocking solution, Dynabeads ® Protein G was added to chromatin/DNA extract containing respective anti-Myc or anti-IgG antibody and incubated at 4℃ overnight. The bead-antibody-chromatin/DNA complexes were collected and washed with Wash Buffer A (20 mM Tris-HCl, pH 8.0, 2 mM EDTA, 1% Triton X-100, 0.1% SDS, 150 mM NaCl), Buffer B (20 mM Tris-HCl, pH 8.0, 2 mM EDTA, 1% Triton X-100, 0.1% SDS, 500 mM NaCl), and Buffer C (10 mM Tris-HCl, pH 8.0, 1 mM EDTA, 1% NP-40, 1% sodium deoxycholate, 0.25M LiCl)

doi:10.6342/NTU202000783

by rotation at RT for 5 min each, repeated three times. These washes were followed with two TE buffer (10 mM Tris-HCl, pH 8.0, 1 mM EDTA) washes at RT for 5 min. Freshly prepared 200 μl elution buffer (0.1 M $NaHCO_3$, 1% SDS) was added to beads, and then incubated for 15 min at 65°C. The elution step was repeated, and buffer was added to final concentrations of 0.2 M NaCl and 0.2 μg/ μl RNase A (Sigma) prior to incubating at 65°C overnight in order to reverse crosslinking of eluted DNA and protein. Input control treated with the same procedure to reverse crosslinking of DNA and protein. Proteins were removed by a final digestion with 0.2 μg/μl proteinase K (Roche) at 65°C overnight. Recovered DNA was purified with QIAquick PCR purification kit (Qiagen), and its concentration was determined using Picogreen (Invitrogen).

To analyze enrichment of respective *fgf3* PAX binding element, PCR was conducted in reaction containing 2 μl purified DNA and respective primer pair (*fgf3* PAX binding element I (PBEI): 5'-GCC AGG GCC CCA AGA CAC T-3' and 5'- CTG CGA GCC GGG GAA CAA AA-3'; *fgf3* PBEII: 5'- TAC TGG ACC TGC ACT TTT CAC CTT-3' and 5'- ACT CCA ATC CTT CAG CAC TAC TCG-3; *cdx1b* non-binding control: 5'- GGG GCC TCG AAG TTT CTG TT-3' and 5'-AGC CCC ATC CGA TCT GGT TA-3'). The PCR program was set as 95℃ 10 min 1 cycle for pre-incubation; amplification set 95℃ 10 sec, 60℃ 10 sec, 72℃ 10 sec for 70 cycles; melting curve 95℃ 5 sec, 40℃ 1 min, from 65℃ 5 sec to 97℃ (Ramp rate 0.02℃/sec) continuous

doi:10.6342/NTU202000783

acquisition (25 acquisitions per ℃), final cooling at 40℃ 30 sec.

2.9 Semi-quantitative reverse-transcription polymerase chain reaction (RT-PCR) and Real-time quantitative reverse-transcription polymerase chain reaction (RT-qPCR)

GoScript™ Reverse Transcription System (Promega) was used for first strand cDNA synthesis. The reaction contained 1 μg total RNA, 0.5 μg oligo (dT) primer and nuclease-free water to final volume 5 μl, heated at 70℃ for 5 min and chilled on ice for at least 5 min. 15 μl reverse transcription reaction mix including final concentration GoScript™ 1x reaction buffer, 0.875 mM $MgCl_2$, 0.5mM dNTP, 20 units Recombinant RNasin® Ribonulease Inhibitor, 1 μl GoScriptTM Reverse Transcriptase and nuclease-free water were added. Program (Annealing at 25℃ for 5 min, extension at 42℃ up to 1 h, and 70℃ for 15 min.) was used for first strand cDNA synthesis.

Semi-quantitative RT-PCR was performed in a 25 μl reaction containing 250 ng cDNA, forward and reverse primer pair (each 10 pmole) of *pax1a* and *pax1b,* and Phusion™ High-Fidelity DNA Polymerase (Finnzymes) using Applied Biosystems Veriti Thermal Cycler. Embryos from 1-cell, shield, bud, 12 hpf and 18 hpf were analyzed using respective primer pair (*pax1a*: 5’- GTG CGC GTA CTC TCC CTC CAA CC -3’ and 5’- TTA AAT AGC CAA CCA CCA AAC AAC -3’; *pax1b*: 5’- CGG CGC AAT CGG TGG GAG TAA -3’ and 5’- AAG TTT GGA GCC GGT GGG TGA CA -3’).

doi:10.6342/NTU202000783

The PCR program was set as 95℃ 10 min 1 cycle for pre-incubation; 95℃ 10 sec, 61.5℃ 15 sec, 72℃ 10 sec for 26 cycles for amplification; 72℃ 7 min for final extension and hold at 4℃.

RT-qPCR was conducted in a 20 μl reaction, containing 20 ng diluted cDNA, forward and reverse primer pair (each 5 pmole) of target gene, LightCycler® 480 SYBR Green I Master mix at 1x final concentration (Roche) and PCR grade water using a Roche Light Cycler 480 II thermal cycler. The PCR program was set as 95℃ 10 min 1 cycle for pre-incubation; amplification set 95℃ 10 sec, 60℃ 10 sec, 72℃ 10 sec for 45 cycles; melting curve 95℃ 5 sec, 40℃ 1 min, from 65℃ 5 sec to 97℃ (Ramp rate 0.02℃/sec) continuous acquisition (25 acquisitions per ℃), final cooling at 40℃ 30 sec.

To analyze *pax1a-201* and *pax1a-202* expression level, RT-qPCR was conducted using total RNA isolated from 24, 48, 72 and 96 hpf wild type embryos for RT reaction and respective primer pair (*pax1a-201*: 5'- GAT TTA GGT CAT GTG TGT TAT ATG-3' and 5'- GCA AGA CAC GAA AGC ATT CAA C-3', which located in 5'UTR and exon1; *pax1a-202*: 5'-CTC CAG CAA ACA TCA CCC TGC-3' and 5'-TCT CTA TGG TAG AAT GGG ACA AG-3', which located in 5'UTR) was used for qPCR reaction. To compare endogenous *pax1b* expression level between wild type and different *Tg(pax1b: eGFP)* genotype, RT-qPCR was conducted using total RNA isolated from 36

doi:10.6342/NTU202000783

hpf wild type, *Tg(pax1b: eGFP)* heterozygous and homozygous embryos for RT reaction and primer pair (*pax1b-201*: 5'-AGC GCA GGT CTC AGT CAT CC-3' and 5'-TGT TCG GTG GTC TTT GTG TTC TTA-3', which located in exon4, exon5 and 3'UTR region) was used for qPCR reaction.

Primer pair (5'-CGA GCA GGA GAT GGG AAC C-3' and 5'-GGG CAA CGG AAA CGC TCA T-3') of *β-actin* was used as control.

2.10 Western blot analysis

Total protein was isolated from 30 embryos at different stages by rinsing with 1x PBS containing 1 mM PMSF (Phenylmethanesulfonyl fluoride, Sigma) and 1x PI (Protease Inhibitor Cocktail tablet, Roche) twice before homogenization in 90 μl 1x RIPA lysis buffer (Millipore) containing 1 mM PMSF and 2x PI by pellet pestles grinding. Extracts were incubated on ice for 30 min and vortexed for 15 seconds every 10 min before centrifugation at 13,000 rpm for 20 min at 4℃. Supernatants were added with equal volume 2x sample buffer (63M Tris-HCl, pH 6.8, 10% glycerol, 0.05% β-mercaptoethanol, 3.5% SDS), boiled for 10 min in water bath and then cooled on ice. They were separated by electrophoresis on 11% SDS-PAGE by loading 30 μl per sample and 5 μl molecular weight marker and later transferred to Immobilon®-P transfer polyvinylidene difluoride (PVDF) membranes (Millipore). PVDF membranes were blocked with 10 ml 1% casein in 1x PBST (137 mM NaCl, 2.68 mM KCl, 1.47

doi:10.6342/NTU202000783

mM KH_2PO_4, 8.1mM Na_2HPO_4, pH 7.4) for 1 h at RT before incubated with first antibody in 1% casein in 1x PBST overnight at 4℃. After PBST wash for 1 h at RT, PVDF membranes were incubated with second antibody in 1% casein in 1x PBST overnight at 4℃. After PBST wash for 1 h at RT, immune-reactive signals were detected by Luminata Crescendo Western HRP Substrate (Millipore) by incubated with 0.5-1 ml HRP substrate for 5 min at RT before scanning using UVP BioSpectrum® 600 Imaging System.

To compare Pax1 expression among 72 hpf wild type, *pax1a*$^{-/-}$ mutant, 0.75 ng *pax1b* MO-injected *pax1a*$^{-/-}$ mutant, *pax1b*$^{-/-}$ mutant, 0.75 ng *pax1a* MO-injected *pax1b*$^{-/-}$ mutant and *pax1a*$^{-/-}$*; pax1b*$^{-/-}$ double mutant, Western blot was conducted using Anti-PAX1 antibody (1:1000, Abcam) as first antibody with anti-α-tubulin (1:5000, Sigma-Aldrich) as control as well as peroxidase-conjugated goat anti-rabbit IgG (1:5000, Jackson) and peroxidase-conjugated goat anti-mouse IgG (1:5000, Jackson) as secondary antibody. High range Prestained SDS-PAGE Standards (Bio-RAD) was used as a molecular weight marker.

To confirm expression of Pax1a-Myc or Pax1b-Myc, Western blot was conducted on total protein isolated from 36 hpf wild type embryos and supernatant of ChIP from 25 pg *pax1a-Myc* plasmid DNA-injected or 25 pg *pax1b-Myc* plasmid DNA-injected 32-36 hpf embryos using anti-Myc-Tag mouse antibody (1:3000, Cell Signaling) as first

doi:10.6342/NTU202000783

antibody with anti-α-tubulin (1:5000, Sigma-Aldrich) as control and peroxidase-conjugated goat anti-mouse IgG (1:5000, Jackson) as second antibody. Amersham full-range rainbow molecular weight marker (Sigma-Aldrich) was used.

2.11 Paraffin sectioning

pax1a or *pax1b* hybridized 36, 48 and 96 hpf embryos were dehydrated in gradient methanol solution (25%, 50%, 75%) with 1x PBS for 10 min per concentration, washed with 100% methanol solution for10 min twice and later washed with 100% isopropanol for 10 min twice. Embryos were incubated with Histo-Clear II (Agar Scientific) for 20 min three times at RT, incubated with solution of wax: Histo-Clear II (1:1) for 30 min at 58℃, and then replaced with wax for 50 min three times at 58℃. The wax filtrated embryos were embedded into paraffin blocks to perform 5 μm series section. Paraffin sections were picked up by microscope slides and dried at 37℃ before deparaffinization and mounting.

2.12 Image acquisition, statistics, and quantification of area

Images of embryos were acquired using an AxioCam HRC camera on a Zeiss Axio Imager M1 microscope equipped with DIC mode. High resolution fluorescent images were captured using a Leica TCS-SP5-MP confocal microscope.

Microsoft Excel was used to perform two-tailed Student's *t*-test with equal or unequal variance. The area within *dlx2a*-labeled pharyngeal arches 3 and 4 were quantified

doi:10.6342/NTU202000783

using ImageJ software as described (Chen et al., 2019). The intensity of semi-quantitative RT-PCR bands was quantified using VisionWorks® Life Science Software by UVP.

doi:10.6342/NTU202000783

3. Results

3.1 zebrafish *pax1a* and *pax1b*

Zebrafish has two *pax1* paralogues, *pax1a* and *pax1b*. Based on recent Genome assembly [GRCz11 (GCA_000002035.4)], *pax1a* is located on Chromosome 17 forward strand, between 42,274,240 and 42,278,340 bps. There are two *pax1a* transcripts, *pax1a-201* and *pax1a-202*, which contain respective four and five exons. They encode respective 359 aa- and 354 aa- long polypeptides and have 5 amino acids difference at the N-terminus. To check embryonic expression level of *pax1a-201* and *pax1a-202*, RT-qPCR was conducted at 24 hpf, 48 hpf, 72 hpf and 96 hpf using primer pairs located in the unique 5'UTR regions (Fig. 1). *pax1a-201* expression level is about half of *pax1a-202*. In this study, we used *pax1a-202* to represent *pax1a* due to its higher expression level. Whereas *pax1b* is located on Chromosome 20 reverse strand, between 48,694,056 and 48,701,593 bps. *pax1b* produces three transcripts, *pax1b-201*, *pax1b-202* and *pax1b-203*, which contains respective five, three and four exons. However, deduced amino acids of protein of *pax1b-202* or *pax1b-203* do not contain predicted ATG codon. We then used *pax1b-201* to represent *pax1b*. Pax1a-202 and Pax1b-201 shares 73.65% amino acid sequence identity using NCBI protein BLAST alignment tool.

3.2 *pax1a* and *pax1b* are co-expressed in pharyngeal pouches

doi:10.6342/NTU202000783

Since zebrafish has two *pax1* paralogues, we first investigated *pax1a* and *pax1b* expression pattern by *in situ* hybridization. In order to understand specific expression pattern of these two genes, we designed the location of *pax1a* and *pax1b* RNA probe in respective 3'UTR and 5'UTR region. Due to failure of *in situ* hybridization for early stage embryos, we then conducted semi-quantitative RT-PCR for samples from 1-cell to 18 hpf and *in situ* hybridization for embryos during 18 to 120 hpf.

Semi-quantitative RT-PCR results indicated that both *pax1a* and *pax1b* are maternal transcripts. Decreased *pax1a* expression was observed during shield and bud stages while *pax1b* expression levels were maintained from shield to 18 hpf as compared with *β-actin* control (Fig. 2A, 3A).

Both *pax1a* and *pax1b* were expressed in the pharyngeal pouches 1 and 2 at 18 hpf (Fig. 2B, 2F, 3B, 3F). Expression of *pax1a* was then detected in pharyngeal pouches 1-3 and the anterior sclerotome at 24 hpf (Fig. 2C,2G). Except anterior sclerotome, *pax1a* expressions were found in pharyngeal pouches 1-4 and 1-5 individual at 30 and 36 hpf (Fig. 2D-E, H-I). From 48 to 120 hpf, *pax1a* transcripts were detected in pharyngeal pouches 1-6 and sclerotome (Fig. 2J-Q). *pax1b* transcript was detected in the pharyngeal pouches 1-3 or pharyngeal pouches 1-4 at 24 and 30 hpf (Fig. 3C, D, G, H). At 36 hpf, *pax1b* was expressed in the pharyngeal pouches 1-5 (Fig, E, I). *pax1b* transcript was detected in the pharyngeal pouches 1-6 during 48 to 120 hpf (Fig. 3J-Q).

doi:10.6342/NTU202000783

Anterior sclerotome expression of *pax1b* could be detected from 36 to 120 hpf (Fig. 3I-Q). These results indicate that both *pax1a* and *pax1b* are mainly expressed in the pharyngeal pouches and their expression in the sclerotome are minimum. Paraffin sectioning of *pax1a*- or *pax1b*- hybridized embryos further indicated the location of signals in different endodermal pouches during 36 to 96 hpf (Fig. 2R-U, 3R-T).

In order to know whether these two genes are expressed in the same region, double fluorescence *in situ* hybridization was performed and demonstrated that *pax1a* and *pax1b* were co-expressed in the pharyngeal pouches at 36 hpf (Fig. 4A-C). We further confirmed endodermal location of *pax1a* and *pax1b* in the pharyngeal arches by double fluorescence *in situ* hybridization using *pax1b* and endodermal (*nkx2.3* and *nkx2.7*) or neural crest (*dlx2a*) marker genes at 36 hpf. *nkx2.3* was co-expressed with *pax1b* in ventral regions of pharyngeal pouches 2-6, while *nkx2.7* was co-expressed with *pax1b* in larger regions of pharyngeal pouches 3-6 (Fig. 4D-I). In contrast, expression of *pax1b* was adjacent to *dlx2a* expressed in the neural crest cells of pharyngeal arches 1-6 (Fig. 4J-L). These observations demonstrate that *pax1b* is expressed in all pharyngeal pouches but not in neural crest cells of pharyngeal arches.

3.3 *Tg(pax1b: eGFP)* enhancer trap fish line expressing eGFP in the developing pharyngeal pouches

A *Tg(pax1b: eGFP)* enhancer trap fish line was derived from a population of fishes

doi:10.6342/NTU202000783

that had been injected with Tol2-Gal4-VP16; UAS: EGFP-Tol2 plasmid. To evaluate whether the insertion of Tol2-Gal4-VP16; UAS: EGFP-Tol2 plasmid in *Tg(pax1b: eGFP)* transgenic embryos affect endogenous *pax1b* expression, RT-qPCR was performed to compare endogenous *pax1b* expression level between WT and *Tg(pax1b: eGFP)* embryos at 36 hpf when all six pharyngeal pouches develop. Compared to wild type embryos, a 1.5-fold increase but 0.4-fold reduction of *pax1b* level was found in heterozygous and homozygous *Tg(pax1b: eGFP)* embryos, respectively (Fig 5).

Double fluorescence *in situ* hybridization showed that *pax1b* was co-expressed with *eGFP* in the pharyngeal pouches at 30 and 36 hpf (Fig. 6A-C). Time-lapse analysis was conducted to investigate the morphogenesis of pharyngeal pouches in *Tg(pax1b: eGFP)* embryos. eGFP expression in the foregut endodermal cells near the midline was detected beginning at 12.5 hpf (Fig. 6H). Pharyngeal pouch 1 emerged, as indicated by intense eGFP expression near the midline at 14 hpf and pharyngeal pouch 2 appeared similarly in the adjacent region at 15 hpf (Fig. 6J, K). Pharyngeal pouch 1 eGFP-positive endodermal cells were seen to migrate laterally and connect with pharyngeal endodermal cells at 16 hpf (Fig. 6L). Pharyngeal pouch 3 then appeared beneath pharyngeal pouch 2 at 18 hpf (Fig. 6M). From 20-22 hpf, endodermal cells of pharyngeal pouch 1-3 continued migrating laterally, and pharyngeal pouch 1 was almost fully formed by 22 hpf (Fig. 6N, O). Pharyngeal pouch 4 emerged beneath pharyngeal

doi:10.6342/NTU202000783

pouch 3 at 24 hpf, and pharyngeal pouch 5 appeared next to pharyngeal pouch 4 at 26 hpf (Fig. 6P, Q). At 28-34 hpf, endodermal cells from pharyngeal pouch 2 gradually condensed, reaching its final form and separating from pharyngeal pouch 1 by 34 hpf. Pharyngeal pouch 3 endodermal cells migrated further laterally, and endodermal cells from pharyngeal pouch 4 and 5 started to migrate laterally beginning at 30 hpf (Fig. 6R-U). Thus, eGFP-positive endodermal cells signify the location of developing pharyngeal pouches prior to their lateral migration.

3.4 Deficiency of *pax1a* and *pax1b* leads to defects in the development of ceratobranchial cartilage and reduced expression of *dlx2a* and *hand2*

To investigate roles of *pax1a* and *pax1b* in zebrafish pharyngeal arch development, we conducted morpholino-mediated knockdown experiments. Translation-blocking morpholinos (MOs) that inhibit protein synthesis of *pax1a* or *pax1b* and corresponding 5 bases- mismatched (5mm) control morpholinos were synthesized (Fig. 7A, B). To test specificity of *pax1a* MO and *pax1b* MO, we inserted 5'UTR and part of coding sequence containing target of *pax1a* or *pax1b* MO into eGFP-pcDNA3 vector. In contrast to embryos co-injected with *pax1a-eGFP-pcDNA3* plasmid and *pax1a* 5mm control MO showing ubiquitous eGFP expression, weak or no eGFP expression were identified in embryos co-injected with *pax1a-eGFP-pcDNA3* plasmid and *pax1a* MO (Fig. 7C, D). Similar eGFP expression reduction level was identified in embryos co-

doi:10.6342/NTU202000783

injected with *pax1b-eGFP-pcDNA3* plasmid and *pax1b* MO (Fig.7E, F).

Mandibular pharyngeal arch 1 (Meckel's cartilage (m) and palatoquadrate (pq)), hyoid pharyngeal arch 2 (hyosymplectic (hs), interhyal (ih), ceratohyal (ch)) and five branchial arches (ceratobranchial (cb), hypobranchial (hb) and basibranchial (bb)) were identified in Alcian blue-stained wild types and embryos injected with 0.75 ng each of 5mm *pax1a* MO and 5mm *pax1b* MO at 96 hpf (Fig. 8A, B). Mild pharyngeal cartilage defects (shortened cb 2-3, lack of cb 1 and 4 on one side, and lack of cb1 on the other side) and two types of severe cartilage defects (straightened ch, shortened cb 2-3, lack of cb 1 and 4 on one side and lack of cb 1-4 on the other side; reversed ch and lack of cb 1- 4 on both sides) were detected in embryos injected with doses of 1.5 ng *pax1a* MO or 10 ng *pax1b* MO (Fig. 8C-G). Notably, the majority of embryos injected with suboptimal doses (0.75 ng) of both *pax1a* MO and *pax1b* MO exhibited severe pharyngeal cartilage defects, indicating that Pax1a and Pax1b have redundant function in the development of pharyngeal cartilages.

We then used CRISPR-Cas9 mutagenesis to generate *pax1a* mutants and *pax1b* mutants. Three sgRNAs each were designed with ZiFIT to target exon 2 of the *pax1a* and *pax1b* genes. All designed sgRNAs were capable to generate indel (insertion and deletion) with different efficiency. Paired box domains of Pax1a and Pax1b proteins are located between 4 to130 amino acids and 6 to 132 amino acids, respectively. We raised

doi:10.6342/NTU202000783

pax1a^{as36} mutant, which carries a 5-bp deletion and is predicted to produce a truncated Pax1a protein with 38 residues. 28 of the 38 amino acids are misframed and no functional paired box domain is present (Fig. 9A, C). We also kept *pax1b*^{as37} mutant, which carries a 5-bp deletion; this mutant is predicted to yield a truncated Pax1b protein of 74 amino acids, 62 of which are misframed and no functional paired box domain (Fig. 9B, D).

Embryos from *pax1a*$^{+/-}$ incrosses exhibited normal pharyngeal cartilages by Alcian blue staining, but after injection with 1.5 ng *pax1b* MO, about 21.1 % of the *pax1a*$^{-/-}$ mutant embryos showed a lack of ceratobranchial cartilage development (Fig. 9E-H). Similarly, normal pharyngeal cartilage was detected in *pax1b*$^{-/-}$ mutant embryos, but a lack of ceratobranchial cartilages and the presence of straight or reversed ch in hyoid arches were identified at 96 hpf in *pax1b*$^{-/-}$ mutant embryos injected with 0.75 ng *pax1a* MO (Fig. 9I-L).

pax1a$^{-/-}$*; pax1b*$^{-/-}$ double mutants were generated, which exhibited a straight vertebral body and normal pectoral fin like wild type embryos but lacked ceratobranchial cartilage and a swim bladder at 96 hpf (Fig. 9M-P). Alcian blue staining of flat-mounted embryos further revealed a loss of ceratobranchial (cb) cartilages 1-4, reduced length of cb 5, absence of basibranchial (bb) cartilages 2-5, absence of all hypobranchial cartilages, and a loss of anterior hyomandibula cartilage (hm) in *pax1a*$^{-/-}$*;*

doi:10.6342/NTU202000783

pax1b$^{-/-}$ double mutants compared to wild-type or *pax1b*$^{-/-}$ mutant embryos at 96 hpf (Fig. 9Q-S).

In order to investigate when pharyngeal arch morphogenesis was first affected in *pax1a*- and *pax1b*-deficient embryos, two marker genes including *hand2* which is expressed in ring of ventral neural crest and *dlx2a* which is expressed in postmigratory neural crests were used (Nair et al., 2007). In *pax1a; pax1b* morphants (co-injected with 0.75 ng each of *pax1a* MO and *pax1b* MO), reduced or absent expression of *hand2* and *dlx2a* was detected in the neural crest of pharyngeal arches 3-5 at 30 hpf (Fig.10 A-H). In addition, reduced or absent expression of *nkx2.3* was identified in *pax1a; pax1b* morphants compared to wild type and control embryos (Fig. 10I-L). Expression of *dlx2a* and *hand2* was also absent in the neural crests of pharyngeal arches 3-6 in the majority of *pax1b*$^{-/-}$ mutants injected with 0.75 ng *pax1a* MO, in contrast to uninjected *pax1b*$^{-/-}$ mutants, wild types, and wild-type embryos injected with 0.75 ng *pax1a* MO at 36 hpf (Fig. 11A-J). Similar defects in expression of *dlx2a* and *hand2* in the neural crests of pharyngeal arches 3-6 were also detected in *pax1a*$^{-/-}$; *pax1b*$^{-/-}$ double mutants compared to sibling controls (i.e., *pax1a*$^{+/-}$; *pax1b*$^{-/-}$ or *pax1a*$^{+/+}$; *pax1b*$^{-/-}$) at 36 hpf (Fig. 11K-N). In *pax1a* MO injected *pax1b*$^{-/-}$ mutants, uninjected *pax1b*$^{-/-}$ mutants, wild types, *pax1a* MO-injected wild types and *pax1a*; *pax1b* morphants, similar *dlx2a* expression levels were observed in three migrating neural crest streams during the 18-20 hpf stages

doi:10.6342/NTU202000783

(Fig. 12A-D, E, F, L, M). However, reduced *dlx2a* expression in the pharyngeal arches 3 and 4 (derived from migrating neural crest stream III) was found at 22 hpf, and absence of *dlx2a* expression in the same pharyngeal arches was noted from 26 hpf in *pax1a*; *pax1b* morphants (Fig. 12 G-K, N-R).

3.5 Evaluation of apoptosis and cell proliferation rate in *pax1a* and *pax1b* deficiency embryos

To address whether cell death or impaired growth might contribute to the absence of *dlx2a* expression in pharyngeal arches 3 and 4, apoptosis and proliferation were assessed. A TUNEL assay was conducted, and similar low levels of apoptotic cells were identified in *dlx2a*-stained pharyngeal arches 3 and 4 of $pax1a^{-/-}$; $pax1b^{-/-}$ double mutants and wild-type embryos at 26 hpf (Fig. 13A-E). Furthermore, no significant difference in the percentage of proliferating neural crest cells, as labeled by anti-PCNA antibody, could be detected in *dlx2a*-stained pharyngeal arches 3 and 4 of $pax1a^{-/-}$; $pax1b^{-/-}$ double mutants and wild-type embryos at the same developmental stage (Fig. 13F-J). In addition, similar low levels of apoptotic cells were identified in *pax1a*-stained pharyngeal pouches 2-5 of $pax1a^{-/-}$; $pax1b^{-/-}$ double mutants and their sibling controls at 36 hpf (Fig. 13K-O). To examine whether deficiency of *pax1a* and *pax1b* contributed to the reduction of *dlx2a* expression in pharyngeal arches 3 and 4at early stage, TUNEL assays were conducted to compare apoptosis between $pax1b^{-/-}$ mutants and $pax1b^{-/-}$

doi:10.6342/NTU202000783

mutant embryos injected with 0.75ng *pax1a* MO at 18, 20 and 22 hpf (Fig. 13P-V). Similar apoptotic cells in third stream neural crests were detected in *pax1a* and *pax1b* deficiency embryos compared to controls during these earlier stages. Moreover, similar apoptotic cells in third stream neural crests were detected in *pax1a*$^{-/-}$; *pax1b*$^{-/-}$ double mutants compared to their sibling controls at 16 hpf (Fig. 13 W-Y).

3.6 Deficiency of *pax1a* and *pax1b* leads to defects in pharyngeal pouch morphogenesis and absence of endodermal expression of *fgf3, tbx1* and *edn1* in pharyngeal pouches

We then evaluated morphogenesis of pharyngeal pouches in *pax1a*$^{-/-}$; *pax1b*$^{-/-}$ double mutants by fluorescence *in situ* hybridization using *pax1a* and *pax1b* probes. Notably, in this experiment, we assumed that transcription of *pax1a* and *pax1b* were not affected by the respective CRISPR-Cas9 mutation. In contrast to sibling control embryos, which exhibited five well-segmented pharyngeal pouches expressing *pax1a* at 36 hpf, *pax1a*$^{-/-}$; *pax1b*$^{-/-}$ double mutant embryos had a segmented *pax1a*-expressing pharyngeal pouch 1 as well as unsegmented pharyngeal pouches 2-5 with continuous *pax1a* expression and small outpocketings (Fig. 14A-C). Similarly, the segmented pharyngeal pouch 1 in *pax1a*$^{-/-}$; *pax1b*$^{-/-}$ double mutant embryos also expressed *pax1b*, and unsegmented pharyngeal pouches 2-5 displayed continuous *pax1b* expression with small outpocketings, while sibling controls had five well-segmented *pax1b*-expressing

doi:10.6342/NTU202000783

pouches (Fig. 14D, E). A lack of *nkx2.3* expression in pharyngeal pouches 2-5 was found in the majority of *pax1b*$^{-/-}$ mutants injected with 0.75 ng *pax1a* MO, in contrast to uninjected *pax1b*$^{-/-}$ mutants, wild types, and wild-type embryos injected with 0.75 ng *pax1a* MO at 36 hpf (Fig. 14F-I). Similar defects in *nkx2.3* expression in pharyngeal pouches 2-6 were also detected in *pax1a*$^{-/-}$; *pax1b*$^{-/-}$ double mutants compared to sibling controls at 36 hpf (Fig. 14J, K). Moreover, no Alcama expression could be detected by zn-5 immunostaining in pharyngeal pouches of *pax1a*$^{-/-}$; *pax1b*$^{-/-}$ double mutants, in contrast with wild-type embryos at 24 and 36 hpf (Fig. 14L-O).

3.7 Pax1a and Pax1b regulate ceratobranchial cartilage formation by modulating expression of *fgf3, tbx1* and *edn1*

Since *pax1a*- and *pax1b*-deficient mutants showed pharyngeal pouch morphogenetic defects like medaka *pax1*-mutant embryos and Fgfs and Tbx1 are known to be essential for morphogenesis of pharyngeal pouches (Choe and Crump, 2014; Crump et al., 2004a; Okada et al., 2016), we next compared expression of *fgf3*, *tbx1* and *edn1* (a downstream effector of Tbx1) in *pax1a*- and *pax1b*-deficient embryos and control embryos. *fgf3* is expressed in the pharyngeal endoderm (Crump et al., 2004b) and *tbx1* expresses is detected in mesodermal core and endodermal epithelia of individual arches (Piotrowski and Nusslein-Volhard, 2000). Expression of *edn1* is detected in the mesodermal cores, ectoderm and endoderm of pharyngeal arches, but not

doi:10.6342/NTU202000783

in NC (Choudhry et al., 2011). In contrast to control embryos, reduced or absent expression of *fgf3*, *tbx1* and *edn1* in pharyngeal pouches 2-4 or 2-5 were detected in *pax1a*; *pax1b* morphants at 30 or 36 hpf (Fig. 15A-X). However, *tbx1* expression in the adjacent mesoderm and *edn1* expression in the mesoderm core of arches 1-3 was not affected. At 36 hpf, a lack of *fgf3*, *tbx1* and *edn1* expression in pharyngeal pouches 2-5 was identified in *pax1a* MO-injected *pax1b*$^{-/-}$ mutants compared to uninjected *pax1b*$^{-/-}$ mutant controls, wild types or *pax1a* MO-injected wild types; meanwhile, *tbx1* expression in the adjacent mesoderm and *edn1* expression in the mesoderm core of arches 1-3 was not affected (Fig. 16 A-L). Similar defects in endodermal expression of *fgf3*, *tbx1* and *edn1* were detected in the pharyngeal pouches of *pax1a*$^{-/-}$; *pax1b*$^{-/-}$ double mutants compared to sibling controls at 36 hpf (Fig. 16 M-R).

We next investigated whether Pax1a/b directly regulates *fgf3* expression. Two conserved PAX1 binding elements were identified in two enhancer regions located 5′ upstream of *fgf3* (-69,697 to -69,448 and -68,981 to -68,869) by the UCSC genome browser (Fig. 17A, B). Initially we evaluated whether Anti-PAX1 antibody from company can recognize endogenous Pax1a or Pax1b protein by Western blot. We isolated total protein from wild type, *pax1a*$^{-/-}$ mutant, *pax1b* MO-injected *pax1a*$^{-/-}$ mutant, *pax1b*$^{-/-}$ mutant, *pax1a* MO-injected *pax1b*$^{-/-}$ mutant and *pax1a*$^{-/-}$; *pax1b*$^{-/-}$ double mutant embryos at 36 hpf for SDS PAGE. Although ~40 kDa protein band which

doi:10.6342/NTU202000783

is close to deduced amino acid number of Pax1a or Pax1b appeared when reacted with Anti-PAX1 antibody, they did not reflect expected protein level in different *Pax1a and Pax1b* deficiency embryos (Fig. 18 A). Since antibodies for zebrafish Pax1a and Pax1b are not available, we performed chromatin immunoprecipitation by overexpressing *pax1a-Myc* and *pax1b-Myc* in 1-2 cell zygotes. Initial Western blot analysis confirmed a protein band with molecular weight 52 kDa (5x Myc about 10 kDa + 38 kDa of Pax1a or 5x Myc about 10 kDa + 37 kDa of Pax1b), two protein bands between 38 and 24 kDa reacted with anti-Myc antibody for total protein isolated from embryos injected with *pax1a-Myc* and *pax1b-Myc* plasmid (Fig. 18 B). We then injected *pax1a-Myc* or *pax1b-Myc* plasmid into 1 cell zygotes and fixed developing embryos at 32-36 hpf. Isolated chromatin was precipitated using anti-Myc antibody or anti-IgG antibody. Three protein bands including expected 52 kDa were only identified in supernatant using anti-IgG antibody but not anti-Myc antibody for immunoprecipitation by Western blot analysis; this indicates Myc-tagged Pax1a or Myc-tagged Pax1b did express in embryos injected with *pax1a-Myc* or *pax1b-Myc* plasmid (Fig. 18 C). Subsequently we performed chromatin immunoprecipitation by overexpressing *pax1b-Myc* in 1-2 cell zygotes. Injected embryos were fixed at 32-36 hpf, and isolated chromatin was precipitated using anti-Myc antibody or anti-IgG antibody. Significant enrichment of qPCR products was observed when using primer pairs to amplify PAX binding element (PBE) I and II, but

doi:10.6342/NTU202000783

no enrichment was observed when using control primer pair for *cdx1b* exon II (Fig. 17 C-E). These results suggest that Pax1b can directly bind to PAX binding elements located in the 5′ upstream region of *fgf3* to activate its transcription.

doi:10.6342/NTU202000783

4. Discussion

In the present study, we used CRISPR-Cas9 mutagenesis and morpholino-mediated knockdown to show that zebrafish Pax1a and Pax1b redundantly regulate the development of pharyngeal pouches and ceratobranchial cartilages. Like medaka *pax1*, zebrafish *pax1a* and *pax1b* are expressed in developing pouches. Time-lapse imaging of *Tg*(*pax1b:eGFP)* transgenic fish was used to further reveal that eGFP-postive endodermal cells mark the location of newly developing pharyngeal pouches before they migrate laterally. Furthermore, unsegmented pharyngeal pouches 2-5 (with continuous expression of *pax1a* or *pax1b* and small outpocketings) were detected in zebrafish *pax1a*$^{-/-}$; *pax1b*$^{-/-}$ double mutant embryos (Fig. 14), indicating Pax1a and Pax1b are essential for segmentation of pharyngeal pouches 2-5. We suspect that similar to medaka Pax1, zebrafish Pax1a and Pax1b may control pharyngeal pouch 2-5 segmentation via indirect downregulation of *pax1a* or *pax1b* transcription in the inter-pouch region. In *pax1a*$^{-/-}$; *pax1b*$^{-/-}$ double mutant embryos, a lack of non-cell autonomous negative regulation of *pax1a* or *pax1b* in the inter-pouch endoderm would result in unsegmented pharyngeal pouches 2-5 with continuous expression of *pax1a* or *pax1b*, much like the phenotype in medaka (Okada et al., 2016). However, in contrast to the developmental defects in the *undulated* mouse vertebral column and abnormalities in the vertebral body and neural arches in medaka *pax1* morphants, development of the

doi:10.6342/NTU202000783

vertebral body was not affected in zebrafish *pax1a*- and *pax1b*-deficient embryos (Fig. 9). This difference may be due to the strong rostral to weak posterior expression pattern of *pax1a* (Fig. 2), in addition to the weak *pax1b* expression in cells within the sclerotome (Fig. 3).

Also similar to the findings in medaka, this phenotype may be attributable to absent expression of *fgf3* and *tbx1* in the pharyngeal pouches (Fig. 16). Although *fgf8a* mutant and *fgf3* morphant embryos possess normal pharyngeal pouches, pouch-forming endodermal cells fail to migrate laterally and distinct pouches are not formed in *fgf8a* and *fgf3* double deficient embryos (Crump et al., 2004a). Based on these observations, it has been hypothesized that there is requirement for Fgf signaling from the lateral mesoderm and ventral hindbrain during segmentation of the pharyngeal endoderm into pharyngeal pouches. In addition to Fgfs, Tbx1 is known to be essential for the morphogenesis of pharyngeal pouches (Choe and Crump, 2014). Notably, while *tbx1* mutant embryos fail to generate outpocketing in pouch-forming endoderm, Alcama expression is retained. Mesodermal Tbx1 is known to promote morphogenesis of pharyngeal pouches via modulation of *wnt11r* and *fgf8a* expression. Consequently, we conclude that like medaka Pax1, zebrafish Pax1a and Pax1b control morphogenesis of pharyngeal pouches via activation of *fgf3* and *tbx1*. Interestingly, Alcama was also not detected in *pax1a*$^{-/-}$; *pax1b*$^{-/-}$ double mutant embryos (Fig. 14), suggesting that zebrafish

doi:10.6342/NTU202000783

Pax1a and Pax1b may regulate *alcama* expression as well.

Pharyngeal cartilage defects, including a lack of ceratobranchial cartilages 1-4 and minor defects in hyoid cartilage (loss of anterior hyomandibula, hyosymplectic and ceratohyal are not fused), were identified in zebrafish mutant embryos deficient in *pax1a* and *pax1b* (Fig. 9) as well as medaka *pax1* mutant embryos (Okada et al., 2016). In addition, zebrafish *pax1a*- and *pax1b*-deficient embryos share similar ceratobranchial cartilage defects with mutants or morphants of *fgf3* or *tbx1* (David et al., 2002; Herzog et al., 2004; Piotrowski et al., 2003). Downregulation of *dlx2a* in the cranial neural crest cells of stream III was detected in *fgf3* morphants and mutants at 24 or 26 hpf, indicating that Fgf3 has an early function of maintaining *dlx2a* expression for the specification and survival of posterior neural crest cells. A reduction of *dlx2a* expression in the branchial arches was also identified in the *tbx1* mutant embryo beginning at 16.5 hpf, suggesting that Tbx1 also participates in the specification and survival of posterior neural crest cells by modulating *dlx2a* expression. Zebrafish Dlx2a is essential for survival of neural crest cells that migrate to the pharyngeal arches (Sperber et al., 2008). Additionally, the *Dlx2* gene is known to play an important role in chondrogenesis as a regulator of cell-cell adhesion during mesenchymal condensation in the branchial arches of chick embryos (McKeown et al., 2005). In zebrafish *pax1a*- and *pax1b*-deficient embryos, reduced *dlx2a* expression in pharyngeal arches 3 and 4 was found at 22 hpf,

doi:10.6342/NTU202000783

and absence of *dlx2a* expression in the same pharyngeal arches was observed beginning at 26 hpf (Fig. 11, 12). As a result, we propose that zebrafish Pax1a and Pax1b may modulate expression of *fgf3* and *tbx1* in pharyngeal pouches to maintain *dlx2a* expression in stream III cranial neural crest cells, allowing for proper development of ceratobranchial cartilage. Although *dlx2a* was also shown to be necessary for neural crest cell survival within the first and second pharyngeal arches at 32 hpf in *dlx2a* morphants (Sperber et al., 2008), we detected similar numbers of TUNEL-stained neural crest cells in pharyngeal arches 3 and 4 when comparing *pax1a*$^{-/-}$; *pax1b*$^{-/-}$ double mutants and wild-type embryos at 26 hpf (Fig. 13). Nevertheless, this result does not preclude the possibility that apoptosis may occur in the cranial neural crest cells of stream III during migration to the pharyngeal arches 3-6 in *pax1a*- and *pax1b*-deficient embryos. Such a possibility will be explored in future studies.

Substantial reductions in expression of *edn1* and *hand2* were detected in the posterior pharyngeal arches 3-5 compared to anterior pharyngeal arches 1-2 of the *tbx1* mutant at 25 or 34 hpf, suggesting that Edn1 and Hand2 are downstream effectors of Tbx1 (Piotrowski et al., 2003). In *suc* mutants, substantial decreases in *hand2* expression were reported in the first and second arch as well as posterior arches (Miller et al., 2000). This observation suggests that Edn1 is non-autonomously required to maintain *hand2* expression in cranial neural crest cells for the specification of ventral

doi:10.6342/NTU202000783

pharyngeal cartilages. Furthermore, Edn1 signaling is required for the dorsal-ventral patterning of pharyngeal arches due to its regulation of *hand2* and *dlx* genes (*dlx2a*, *dlx5a*, *dlx3b*, *dlx6a*), which are expressed in gradients along the axis (Walker et al., 2006). Edn1 interacts with EdnrA/B to regulate *hand2* expression in the ventral domain of early arches at 24 hpf, an action that is mediated by modulation of *dlx5*/*dlx6* expression (Medeiros and Crump, 2012). In zebrafish *pax1a*- and *pax1b*-deficient embryos, a lack of *tbx1* and *edn1* expression was found in pharyngeal pouches 2-5, and *hand2* expression was absent in pharyngeal arches 3-6 (Fig. 11, 16). Therefore, we propose that zebrafish Pax1a and Pax1b may regulate expression of *tbx1*, which in turn modulates expression of effectors (*edn1* and *hand2*) for proper development of ceratobranchial cartilage. Besides the ceratobranchial cartilage defect, a loss of the anterior half of hyomandibula cartilage in the hyoid cartilage was observed in *pax1a*$^{-/-}$; *pax1b*$^{-/-}$ double mutants (Fig. 9), similar to the phenotypes observed in *integrinα5* and *fgf8a* mutants (Crump et al., 2004a; Crump et al., 2004b). Like these mutants, *pax1a*$^{-/-}$; *pax1b*$^{-/-}$ double mutants exhibited morphogenetic defects in pharyngeal pouch 1, likely meaning that *integrinα5* signals could not be properly generated in the first pouch to stabilize neural crest cells of the anterior hyomandibula in the adjacent hyoid cartilage.

In addition, we noticed that endogenous *pax1b* expression was increased in heterozygous but decreased in homozygous *Tg(pax1b: eGFP)* embryos compared to

doi:10.6342/NTU202000783

wild type embryos (Fig 5). This observation is partly consistent with previous finding that the insertion of a Tol2 transposon-mediated gene trap construct interfere with endogenous transcript of trapped gene (Kawakami et al., 2004). We considered that the insertion of Tol2-Gal4-VP16; UAS: EGFP-Tol2 plasmid in the 3'UTR of *pax1b* gene may inhibit transcription of endogenous *pax1b* mRNA in homozygous *Tg(pax1b: eGFP)* embryos. However, it is not clear why endogenous *pax1b* transcription was not affected in heterozygous *Tg(pax1b: eGFP)* embryos as well. We also noticed that *pax1a*$^{-/-}$*; pax1b*$^{-/-}$ double mutants lacked an inflated swim bladder at 96 hpf (Fig. 9I-L). A previous study indicated that the inflation of swim bladder was affected in zebrafish embryos treated with a thyroid peroxidase inhibitor or knockdown of iodothyronine deiodinase, which is required to activate T4 into biologically active T3 form (Stinckens et al., 2016). Organogenesis of thymus and thyroid is conserved between mammals and zebrafish; thyroid gland is derived from precursors evaginated from the ventral floor of the pharynx. In contrast to mammalian thyroid gland is enclosed by connective tissue, thyroid follicles of teleosts are loosely distributed along the ventral aorta in the lower jaw region. In zebrafish larvae, T4 immunostaining showed that some non-follicular T4 domains were located ventral to the anterior basibranchial cartilage while later appearing thyroid follicles were distributed along the ventral aorta (Wendl et al., 2002). Therefore, we considered that lack of inflated swim bladder in *pax1a*$^{-/-}$*; pax1b*$^{-/-}$ double

doi:10.6342/NTU202000783

mutant embryos may be attributed to failure of development or function of thyroid follicular cells. To answer this speculation, we can compare expression level of *hhex*, *nk2.1a* and pax2.1 which are required for differentiation or growth of thyroid follicular cells and analyze level of T4 and T3 in *pax1a*$^{-/-}$*; pax1b*$^{-/-}$ double mutants and wild type embryos (Elsalini et al., 2003; Wendl et al., 2002). Interestingly, mouse *Pax1* is also expressed in the third pharyngeal endodermal pouch, from which thymus epithelium is derived, and it is later expressed in the adult thymus, where it is required for thymocyte maturation into T lymphocytes (Wallin et al., 1996). In *pax1* medaka mutants, thymus-specific expression of *foxN1* was also lost (Okada et al., 2016). We can also evaluate *foxn1* gene expression in *pax1a*$^{-/-}$*; pax1b*$^{-/-}$ double mutant embryos to understand whether thymus development is also affected.

doi:10.6342/NTU202000783

5. Conclusion

In conclusion, zebrafish Pax1a and Pax1b have overlapping function in the modulation of proper morphogenesis of pharyngeal pouches and ceratobranchial cartilage formation (Fig. 19). Zebrafish Pax1a and Pax1b act as an upstream integrator, modulating expression of *fgf3* and *tbx1* in pharyngeal pouches. Fgf3 signaling and Tbx1 are known to regulate *dlx2a* expression in the neural crest cells, as an essential action for neural crest differentiation and chondrogenesis. Tbx1 is also known to regulate expression of *edn1*, which then interacts with EdnrA/B in neural crest cells to modulate expression of downstream genes essential for neural crest differentiation and cartilage formation (i.e., *hand2*, *dlx3b*, *dlx5a*, and *dlx6a*). In zebrafish *pax1a*- and *pax1b*-deficient embryos, downregulation of *fgf3*, *tbx1* and *edn1* in the pharyngeal pouches as well as an absence of *dlx2a* and *hand2* expression in the developing posterior pharyngeal arches result in a lack of ceratobranchial cartilage formation. Together with previous findings, our data provide a more complete understanding of the molecular circuitries controlling pharyngeal cartilage development from pharyngeal endodermal pouches in zebrafish.

doi:10.6342/NTU202000783

Alexander, J., Rothenberg, M., Henry, G. L. and Stainier, D. Y. R. (1999). casanova Plays an Early and Essential Role in Endoderm Formation in Zebrafish. *Developmental Biology* **215**, 343-357.

Balling, R., Deutsch, U. and Gruss, P. (1988). undulated, a mutation affecting the development of the mouse skeleton, has a point mutation in the paired box of Pax 1. *Cell* **55**, 531-535.

Barriga, E. H., Maxwell, P. H., Reyes, A. E. and Mayor, R. (2013). The hypoxia factor Hif-1α controls neural crest chemotaxis and epithelial to mesenchymal transition. *Journal of Cell Biology* **201**, 759-776.

Chen, Y. C., Liao, B. K., Lu, Y. F., Liu, Y. H., Hsieh, F. C., Hwang, P. P. and Hwang, S. L. (2019). Zebrafish Klf4 maintains the ionocyte progenitor population by regulating epidermal stem cell proliferation and lateral inhibition. *PLOS Genetics* **15**, e1008058.

Cheung, M., Chaboissier, M. C., Mynett, A., Hirst, E., Schedl, A. and Briscoe, J. (2005). The transcriptional control of trunk neural crest induction, survival, and delamination. *Developmental Cell* **8**, 179-192.

Choe, C. P. and Crump, J. G. (2014). Tbx1 controls the morphogenesis of pharyngeal pouch epithelia through mesodermal Wnt11r and Fgf8a. *Development* **141**, 3583-3593.

Choudhry, P., Joshi, D., Funke, B. and Trede, N. (2011). Alcama mediates Edn1 signaling during zebrafish cartilage morphogenesis. *Developmental Biology* **349**, 483-493.

Crump, J. G., Maves, L., Lawson, N. D., Weinstein, B. M. and Kimmel, C. B. (2004a). An essential role for Fgfs in endodermal pouch formation influences later craniofacial skeletal patterning. *Development* **131**, 5703-5716.

Crump, J. G., Swartz, M. E. and Kimmel, C. B. (2004b). An integrin-dependent role of pouch endoderm in hyoid cartilage development. *PLOS Biology* **2**, E244.

David, N. B., Saint-Etienne, L., Tsang, M., Schilling, T. F. and Rosa, F. M. (2002). Requirement for endoderm and FGF3 in ventral head skeleton formation. *Development* **129**, 4457-4468.

Davison, J. M., Akitake, C. M., Goll, M. G., Rhee, J. M., Gosse, N., Baier, H., Halpern, M. E., Leach, S. D. and Parsons, M. J. (2007). Transactivation from Gal4-VP16 transgenic insertions for tissue-specific cell labeling and ablation in zebrafish. *Developmental Biology* **304**, 811-824.

Dottori, M., Gross, M. K., Labosky, P. and Goulding, M. (2001). The winged-helix transcription factor Foxd3 suppresses interneuron differentiation and promotes neural crest cell fate. *Development* **128**, 4127-4138.

Ferronha, T., Rabadan, M. A., Gil-Guinon, E., Le Dreau, G., de Torres, C. and

doi:10.6342/NTU202000783

Marti, E. (2013). LMO4 is an essential cofactor in the Snail2-mediated epithelial-to-mesenchymal transition of neuroblastoma and neural crest cells. *The Journal of neuroscience : the official journal of the Society for Neuroscience* **33**, 2773-2783.

Gendron-Maguire, M., Mallo, M., Zhang, M. and Gridley, T. (1993). Hoxa-2 mutant mice exhibit homeotic transformation of skeletal elements derived from cranial neural crest. *Cell* **75**, 1317-1331.

Grammatopoulos, G. A., Bell, E., Toole, L., Lumsden, A. and Tucker, A. S. (2000). Homeotic transformation of branchial arch identity after Hoxa2 overexpression. *Development* **127**, 5355.

Grocott, T., Tambalo, M. and Streit, A. (2012). The peripheral sensory nervous system in the vertebrate head: a gene regulatory perspective. *Developmental Biology* **370**, 3-23.

Herzog, W., Sonntag, C., von der Hardt, S., Roehl, H. H., Varga, Z. M. and Hammerschmidt, M. (2004). Fgf3 signaling from the ventral diencephalon is required for early specification and subsequent survival of the zebrafish adenohypophysis. *Development* **131**, 3681-3692.

Hunt, P., Gulisano, M., Cook, M., Sham, M.-H., Faiella, A., Wilkinson, D., Boncinelli, E. and Krumlauf, R. (1991). A distinct Hox code for the branchial region of the vertebrate head. *Nature* **353**, 861-864.

Hunter, M. P. and Prince, V. E. (2002). Zebrafish hox paralogue group 2 genes function redundantly as selector genes to pattern the second pharyngeal arch. *Developmental Biology* **247**, 367-389.

Jao, L. E., Wente, S. R. and Chen, W. (2013). Efficient multiplex biallelic zebrafish genome editing using a CRISPR nuclease system. *Proceedings of the National Academy of Sciences of the United States of America* **110**, 13904-13909.

Kawakami, K., Takeda, H., Kawakami, N., Kobayashi, M., Matsuda, N. and Mishina, M. (2004). A transposon-mediated gene trap approach identifies developmentally regulated genes in zebrafish. *Developmental Cell* **7**, 133-144.

Khudyakov, J. and Bronner-Fraser, M. (2009). Comprehensive spatiotemporal analysis of early chick neural crest network genes. *Developmental Dynamics* **238**.

Kimmel, C. B., Ballard, W. W., Kimmel, S. R., Ullmann, B. and Schilling, T. F. (1995). Stages of embryonic development of the zebrafish. *Developmental Dynamics* **203**, 253-310.

Kitazawa, T., Fujisawa, K., Narboux-Neme, N., Arima, Y., Kawamura, Y., Inoue, T., Wada, Y., Kohro, T., Aburatani, H., Kodama, T., et al. (2015). Distinct effects of Hoxa2 overexpression in cranial neural crest populations reveal that

doi:10.6342/NTU202000783

the mammalian hyomandibular-ceratohyal boundary maps within the styloid process. *Developmental Biology* **402**, 162-174.

Knight, R. D. and Schilling, T. F. (2006). Cranial neural crest and development of the head skeleton. *Advances in experimental medicine and biology* **589**, 120-133.

Labosky, P. A. and Kaestner, K. H. (1998). The winged helix transcription factor Hfh2 is expressed in neural crest and spinal cord during mouse development. *Mechanisms of Development* **76**, 185-190.

LaMonica, K., Ding, H. L. and Artinger, K. B. (2015). prdm1a functions upstream of itga5 in zebrafish craniofacial development. *Genesis* **53**, 270-277.

Liu, J. A., Wu, M. H., Yan, C. H., Chau, B. K., So, H., Ng, A., Chan, A., Cheah, K. S., Briscoe, J. and Cheung, M. (2013a). Phosphorylation of Sox9 is required for neural crest delamination and is regulated downstream of BMP and canonical Wnt signaling. *Proceedings of the National Academy of Sciences of the United States of America* **110**, 2882-2887.

Liu, X., Wang, H., Li, G., Huang, H. Z. and Wang, Y. Q. (2013b). The function of DrPax1b gene in the embryonic development of zebrafish. *Genes & Genetic Systems* **88**, 261-269.

McGaughran, J. M., Oates, A., Donnai, D., Read, A. P. and Tassabehji, M. (2003). Mutations in PAX1 may be associated with Klippel-Feil syndrome. *European Journal of Human Genetics* **11**, 468-474.

McKeown, S. J., Newgreen, D. F. and Farlie, P. G. (2005). Dlx2 over-expression regulates cell adhesion and mesenchymal condensation in ectomesenchyme. *Developmental Biology* **281**, 22-37.

Medeiros, D. M. and Crump, J. G. (2012). New perspectives on pharyngeal dorsoventral patterning in development and evolution of the vertebrate jaw. *Developmental Biology* **371**, 121-135.

Meulemans, D. and Bronner-Fraser, M. (2004). Gene-regulatory interactions in neural crest evolution and development. *Developmental Cell* **7**, 291-299.

Miller, C. T., Schilling, T. F., Lee, K., Parker, J. and Kimmel, C. B. (2000). sucker encodes a zebrafish Endothelin-1 required for ventral pharyngeal arch development. *Development* **127**, 3815-3828.

Miller, C. T., Yelon, D., Stainier, D. Y. and Kimmel, C. B. (2003). Two endothelin 1 effectors, hand2 and bapx1, pattern ventral pharyngeal cartilage and the jaw joint. *Development* **130**, 1353-1365.

Minoux, M. and Rijli, F. M. (2010). Molecular mechanisms of cranial neural crest cell migration and patterning in craniofacial development. *Development* **137**, 2605.

Mise, T., Iijima, M., Inohaya, K., Kudo, A. and Wada, H. (2008). Function of Pax1 and Pax9 in the sclerotome of medaka fish. *Genesis* **46**, 185-192.

doi:10.6342/NTU202000783

Monsoro-Burq, A. H. (2015). PAX transcription factors in neural crest development. *Seminars in Cell and Developmental Biologyl* **44**, 87-96.

Mork, L. A. and Crump, J. G. (2015). Zebrafish Craniofacial Development: A Window into Early Patterning. *Current Topics in Developmental Biology* **115**, 235-269.

Nair, S., Li, W., Cornell, R. and Schilling, T. F. (2007). Requirements for Endothelin type-A receptors and Endothelin-1 signaling in the facial ectoderm for the patterning of skeletogenic neural crest cells in zebrafish. *Development* **134**, 335-345.

Nichane, M., Ren, X., Souopgui, J. and Bellefroid, E. (2008). Hairy2 functions through both DNA-binding and non DNA-binding mechanisms at the neural plate border in Xenopus. *Developmental Biology* **322**, 368-380.

Okada, K., Inohaya, K., Mise, T., Kudo, A., Takada, S. and Wada, H. (2016). Reiterative expression of pax1 directs pharyngeal pouch segmentation in medaka. *Development* **143**, 1800-1810.

Parker, H. J., Bronner, M. E. and Krumlauf, R. (2016). The vertebrate Hox gene regulatory network for hindbrain segmentation: Evolution and diversification: Coupling of a Hox gene regulatory network to hindbrain segmentation is an ancient trait originating at the base of vertebrates. *BioEssays : News and Reviews in Molecular, Cellular and Developmental Biology* **38**, 526-538.

Pasqualetti, M., Ori, M., Nardi, I. and Rijli, F. M. (2000). Ectopic Hoxa2 induction after neural crest migration results in homeosis of jaw elements in Xenopus. *Development* **127**, 5367.

Peters, H., Wilm, B., Sakai, N., Imai, K., Maas, R. and Balling, R. (1999). Pax1 and Pax9 synergistically regulate vertebral column development. *Development* **126**, 5399-5408.

Piotrowski, T., Ahn, D. G., Schilling, T. F., Nair, S., Ruvinsky, I., Geisler, R., Rauch, G. J., Haffter, P., Zon, L. I., Zhou, Y., et al. (2003). The zebrafish van gogh mutation disrupts tbx1, which is involved in the DiGeorge deletion syndrome in humans. *Development* **130**, 5043-5052.

Piotrowski, T. and Nusslein-Volhard, C. (2000). The endoderm plays an important role in patterning the segmented pharyngeal region in zebrafish (Danio rerio). *Developmental Biology* **225**, 339-356.

Pohl, E., Aykut, A., Beleggia, F., Karaca, E., Durmaz, B., Keupp, K., Arslan, E., Palamar, M., Yigit, G., Ozkinay, F., et al. (2013). A hypofunctional PAX1 mutation causes autosomal recessively inherited otofaciocervical syndrome. *Human Genetics* **132**, 1311-1320.

Rodrigo, I., Hill, R. E., Balling, R., Munsterberg, A. and Imai, K. (2003). Pax1 and

doi:10.6342/NTU202000783

Pax9 activate Bapx1 to induce chondrogenic differentiation in the sclerotome. *Development* **130**, 473-482.

Rogers, C. D., Saxena, A. and Bronner, M. E. (2013). Sip1 mediates an E-cadherin-to-N-cadherin switch during cranial neural crest EMT. *Journal of Cell Biology* **203**, 835-847.

Sanchez, R. S. and Sanchez, S. S. (2013). Characterization of pax1, pax9, and uncx sclerotomal genes during Xenopus laevis embryogenesis. *Developmental Dynamics* **242**, 572-579.

Sato, S., Ikeda, K., Shioi, G., Ochi, H., Ogino, H., Yajima, H. and Kawakami, K. (2010). Conserved expression of mouse Six1 in the pre-placodal region (PPR) and identification of an enhancer for the rostral PPR. *Developmental Biology* **344**, 158-171.

Schier, A. F. and Shen, M. M. (2000). Nodal signalling in vertebrate development. *Nature* **403**, 385-389.

Schilling, T. F. and Kimmel, C. B. (1997). Musculoskeletal patterning in the pharyngeal segments of the zebrafish embryo. *Development* **124**, 2945-2960.

Schilling, T. F., Piotrowski, T., Grandel, H., Brand, M., Heisenberg, C. P., Jiang, Y. J., Beuchle, D., Hammerschmidt, M., Kane, D. A., Mullins, M. C., et al. (1996). Jaw and branchial arch mutants in zebrafish I: branchial arches. *Development* **123**, 329-344.

Simões-Costa, M. S., McKeown, S. J., Tan-Cabugao, J., Sauka-Spengler, T. and Bronner, M. E. (2012). Dynamic and Differential Regulation of Stem Cell Factor FoxD3 in the Neural Crest Is Encrypted in the Genome. *PLOS Genetics* **8**, e1003142.

Simoes-Costa, M. and Bronner, M. E. (2015). Establishing neural crest identity: a gene regulatory recipe. *Development* **142**, 242-257.

Southard-Smith, E. M., Kos, L. and Pavan, W. J. (1998). Sox10 mutation disrupts neural crest development in Dom Hirschsprung mouse model. *Nature Genetics* **18**, 60-64.

Sperber, S. M., Saxena, V., Hatch, G. and Ekker, M. (2008). Zebrafish dlx2a contributes to hindbrain neural crest survival, is necessary for differentiation of sensory ganglia and functions with dlx1a in maturation of the arch cartilage elements. *Developmental Biology* **314**, 59-70.

Streit, A., Berliner, A. J., Papanayotou, C., Sirulnik, A. and Stern, C. D. (2000). Initiation of neural induction by FGF signalling before gastrulation. *Nature* **406**, 74-78.

Takimoto, A., Mohri, H., Kokubu, C., Hiraki, Y. and Shukunami, C. (2013). Pax1 acts as a negative regulator of chondrocyte maturation. *Experimental Cell*

doi:10.6342/NTU202000783

Research **319**, 3128-3139.

Taneyhill, L. A., Coles, E. G. and Bronner-Fraser, M. (2007). Snail2 directly represses cadherin6B during epithelial-to-mesenchymal transitions of the neural crest. *Development* **134**, 1481.

Thisse, C. and Thisse, B. (2008). High-resolution in situ hybridization to whole-mount zebrafish embryos. *Nature Protocols* **3**, 59-69.

Timmons, P. M., Wallin, J., Rigby, P. W. and Balling, R. (1994). Expression and function of Pax 1 during development of the pectoral girdle. *Development* **120**, 2773-2785.

Underhill, D. A. (2000). Genetic and biochemical diversity in the Pax gene family. *Biochemistry and Cell Biology / Biochimie et Biologie Cellulaire* **78**, 629-638.

Urasaki, A., Morvan, G. and Kawakami, K. (2006). Functional dissection of the Tol2 transposable element identified the minimal cis-sequence and a highly repetitive sequence in the subterminal region essential for transposition. *Genetics* **174**, 639-649.

Wahlbuhl, M., Reiprich, S., Vogl, M. R., Bosl, M. R. and Wegner, M. (2012). Transcription factor Sox10 orchestrates activity of a neural crest-specific enhancer in the vicinity of its gene. *Nucleic Acids Research* **40**, 88-101.

Walker, M. B., Miller, C. T., Coffin Talbot, J., Stock, D. W. and Kimmel, C. B. (2006). Zebrafish furin mutants reveal intricacies in regulating Endothelin1 signaling in craniofacial patterning. *Developmental Biology* **295**, 194-205.

Wallin, J., Eibel, H., Neubuser, A., Wilting, J., Koseki, H. and Balling, R. (1996). Pax1 is expressed during development of the thymus epithelium and is required for normal T-cell maturation. *Development* **122**, 23-30.

Walshe, J. and Mason, I. (2003a). Fgf signalling is required for formation of cartilage in the head. *Developmental Biology* **264**, 522-536.

Walshe, J. and Mason, I. (2003b). Unique and combinatorial functions of Fgf3 and Fgf8 during zebrafish forebrain development. *Development* **130**, 4337-4349.

Wilm, B., Dahl, E., Peters, H., Balling, R. and Imai, K. (1998). Targeted disruption of Pax1 defines its null phenotype and proves haploinsufficiency. *Proceedings of the National Academy of Sciences of the United States of America* **95**, 8692-8697.

Yelick, P. C. and Schilling, T. F. (2002). Molecular dissection of craniofacial development using zebrafish. *Critical Reviews in Oral Biology and Medicine : an Official Publication of the American Association of Oral Biologists* **13**, 308-322.

Zhang, L., Zhong, T., Wang, Y., Jiang, Q., Song, H. and Gui, Y. (2006). TBX1, a DiGeorge syndrome candidate gene, is inhibited by retinoic acid. *The*

doi:10.6342/NTU202000783

International Journal of Developmental Biology **50**, 55-61.

doi:10.6342/NTU202000783

Figures

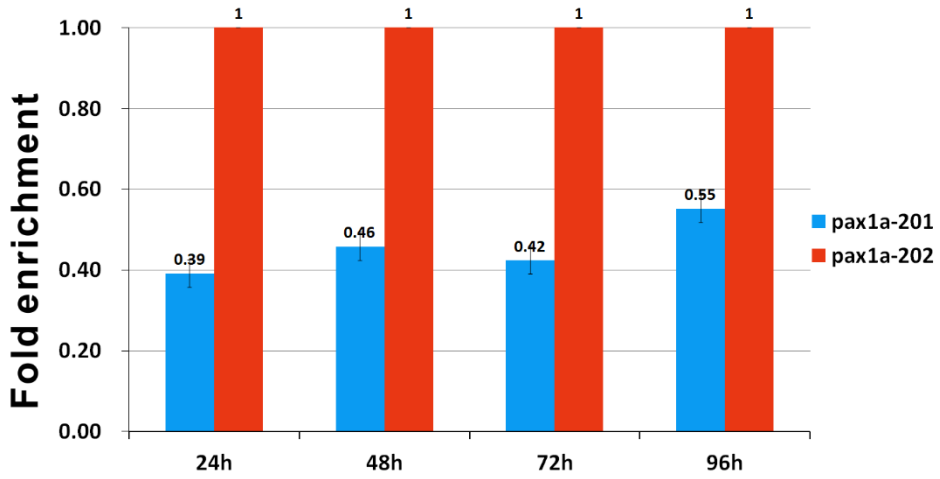

Fig. 1. Embryonic expression level of *pax1a-201* and *pax1a-202*. Expression level of *pax1a-201* (red) and *pax1a-202* (blue) were evaluated by RT-qPCR at 24, 48, 72 and 96 hpf. Expression level of *pax1a-201* is roughly half of *pax1a-202* at these stages.

doi:10.6342/NTU202000783

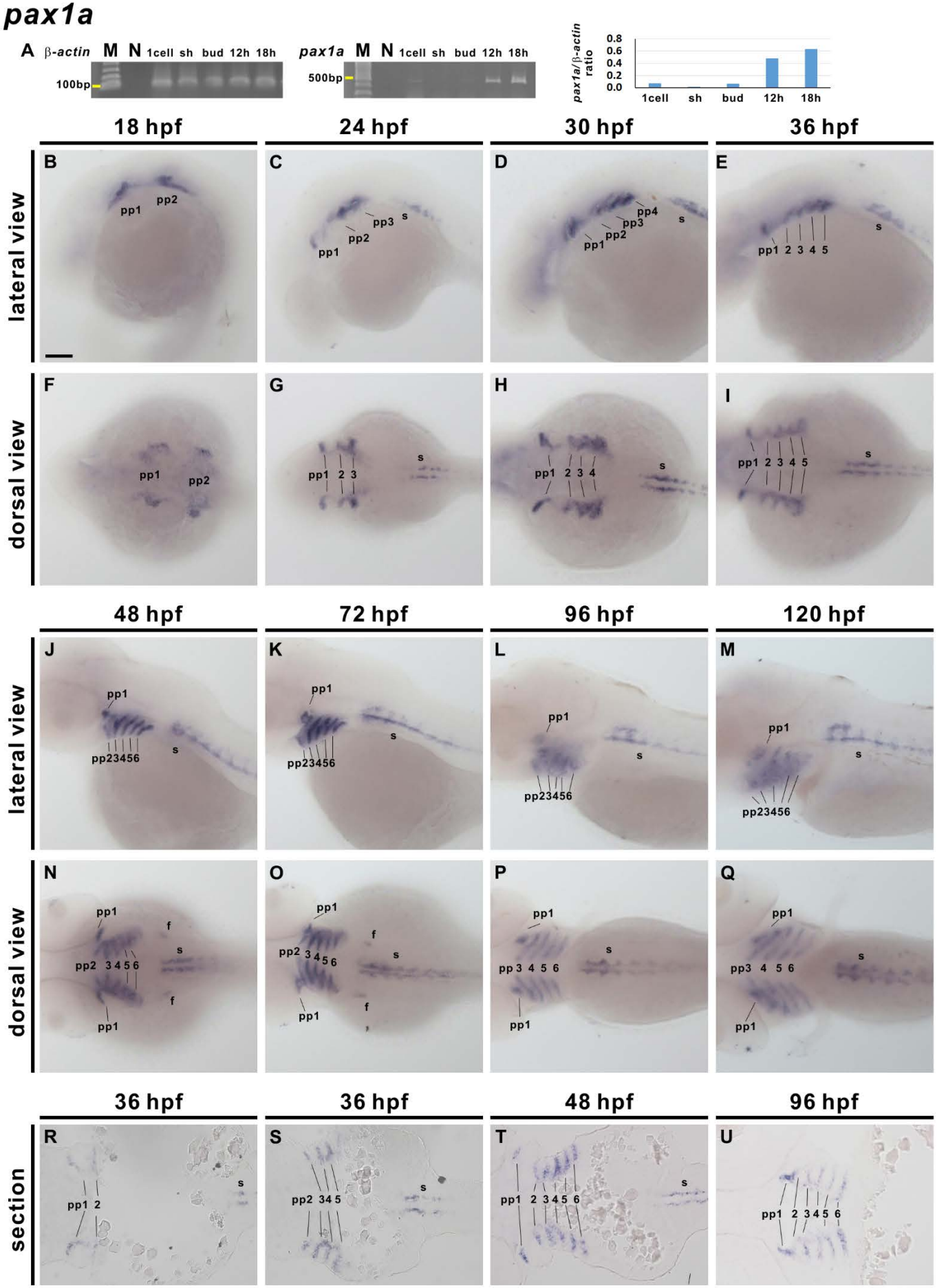

doi:10.6342/NTU202000783

Fig. 2. Developmental expression patterns of zebrafish *pax1a* gene. (A) Semi-quantitative RT-PCR indicates expression of *pax1a* from 1 cell to 18 hpf stages. Expression of *β-actin* was used as a control. Quantitation of *pax1a*/*α-actin* band intensity ratio from 1-cell to 18 hpf stages is shown. M, molecular weight marker; N, no template control. (B-Q) Signals for *pax1a* was detected by *in situ* hybridization in the developing pharyngeal pouches (pp) and sclerotome (s) from 18 to 120 hpf. Embryos in lateral or dorsal view are shown from 18 hpf (B, F), 24 hpf (C, G), 30 hpf (D, H), 36 hpf (E, I), 48 hpf (J, N), 72 hpf (K, O), 96 hpf (L, P) and 120 hpf (M, Q). Paraffin sections of a *pax1a* hybridized embryo shows *pax1a* signal in different pharyngeal pouches (pp) at 36 hpf (R, S), 48 hpf (T) and 96 hpf (U). sh, shield. Scale bar represents 100 μm.

doi:10.6342/NTU202000783

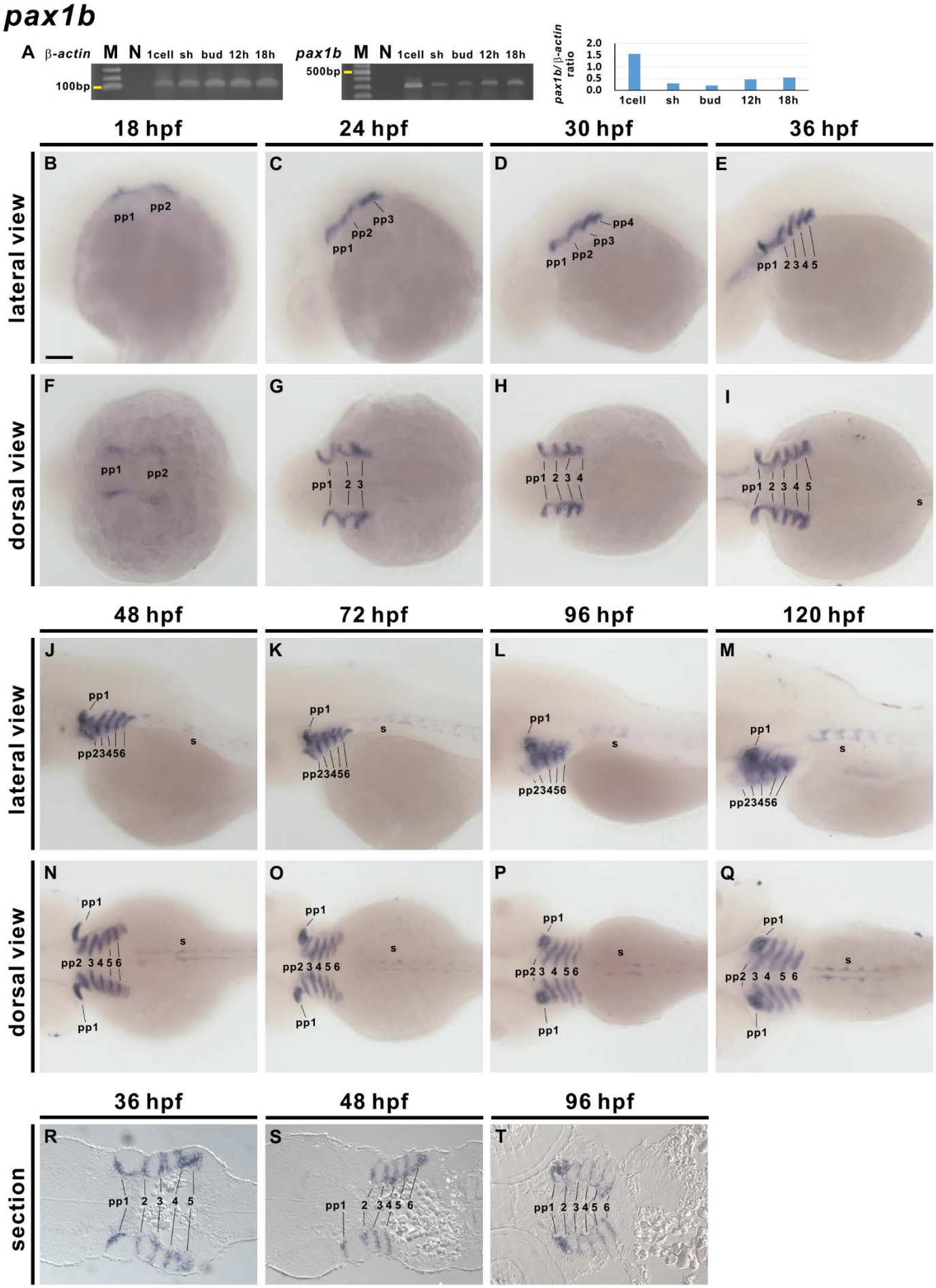

doi:10.6342/NTU202000783

Fig. 3. Developmental expression patterns of zebrafish *pax1b* gene. (A) Semi-quantitative RT-PCR indicates expression of *pax1b* from 1 cell to 18 hpf stages. Expression of *β-actin* was used as a control. M, molecular weight marker; N, no template control. Quantitation of *pax1a/α-actin* band intensity ratio from 1-cell to 18 hpf stages is shown. (B-Q) *pax1b* is expressed in the developing pharyngeal pouches (pp) and sclerotome (s) from 18 to 120 hpf by *in situ* hybridization. Embryos in lateral view or dorsal view are shown from 18 hpf (B, F), 24 hpf (C, G), 30 hpf (D, H), 36 hpf (E, I), 48 hpf (J, N), 72 hpf (K, O), 96 hpf (L, P) and 120 hpf (M, Q). Paraffin sections of a *pax1b* hybridized embryo showed signals locates in different endodermal pouches during at 36 hpf (R), 48 hpf (S) and 96 hpf (T). sh, shield. Scale bars represent 100 μm.

doi:10.6342/NTU202000783

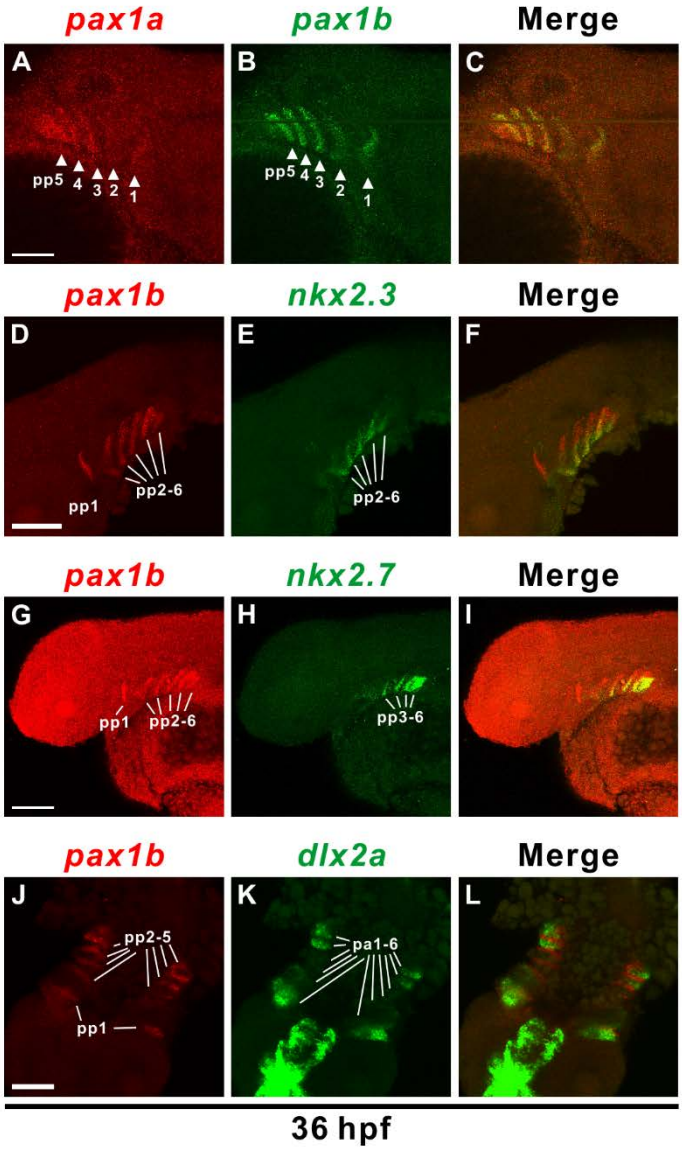

Fig. 4. *pax1b* is expressed in pharyngeal pouches but not in the neural crest cells of pharyngeal arches. (A-C) Double fluorescence *in situ* hybridization revealed co-expression of *pax1a* (A, red) and *pax1b* (B, greed) in pharyngeal pouches 1-5 at 36 hpf. Merged image (C) is shown. Lateral view of embryos is shown with anterior to the right. (D-F) Double fluorescence *in situ* hybridization indicated *pax1b* (D, red) is co-expressed with *nkx2.3* (E, green) in pharyngeal pouches (pp) 2-6 (F, merge) at 36 hpf. (G-H) *pax1b* (G, red) is also co-expressed with *nkx2.7* (H, green) in pharyngeal pouches 3-6 (I, merge). (J-L) Expression of *pax1b* (J, red) in the pharyngeal pouches is adjacent to *dlx2a* (K, green), which is expressed in the neural crest cells of pharyngeal arches (pa). Relative localization is apparent in the merged image (L). Scale bars represent 100 μm.

doi:10.6342/NTU202000783

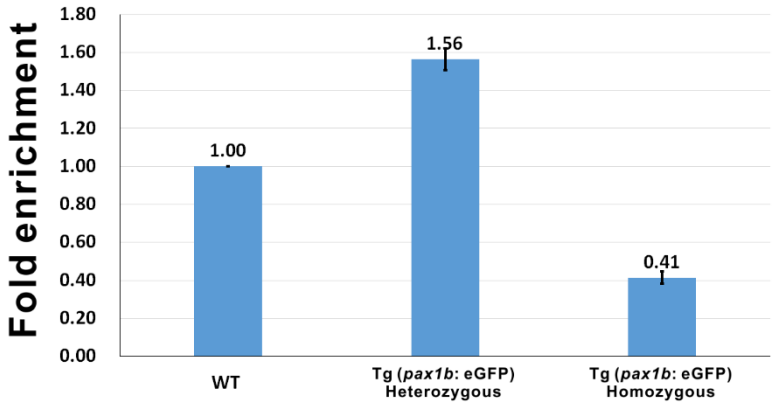

Fig. 5. Comparison of *pax1b* expression level between wild type and *Tg (pax1b: eGFP)* embryos. RT-qPCR was conducted. Compared to wild type embryos, a 1.5 fold increase of *pax1b* level was identified in heterozygous *Tg (pax1b: eGFP)* embroyos while a 0.4 fold reduction of *pax1b* level was detected inhomozygous *Tg (pax1b: eGFP)* embroyos.

doi:10.6342/NTU202000783

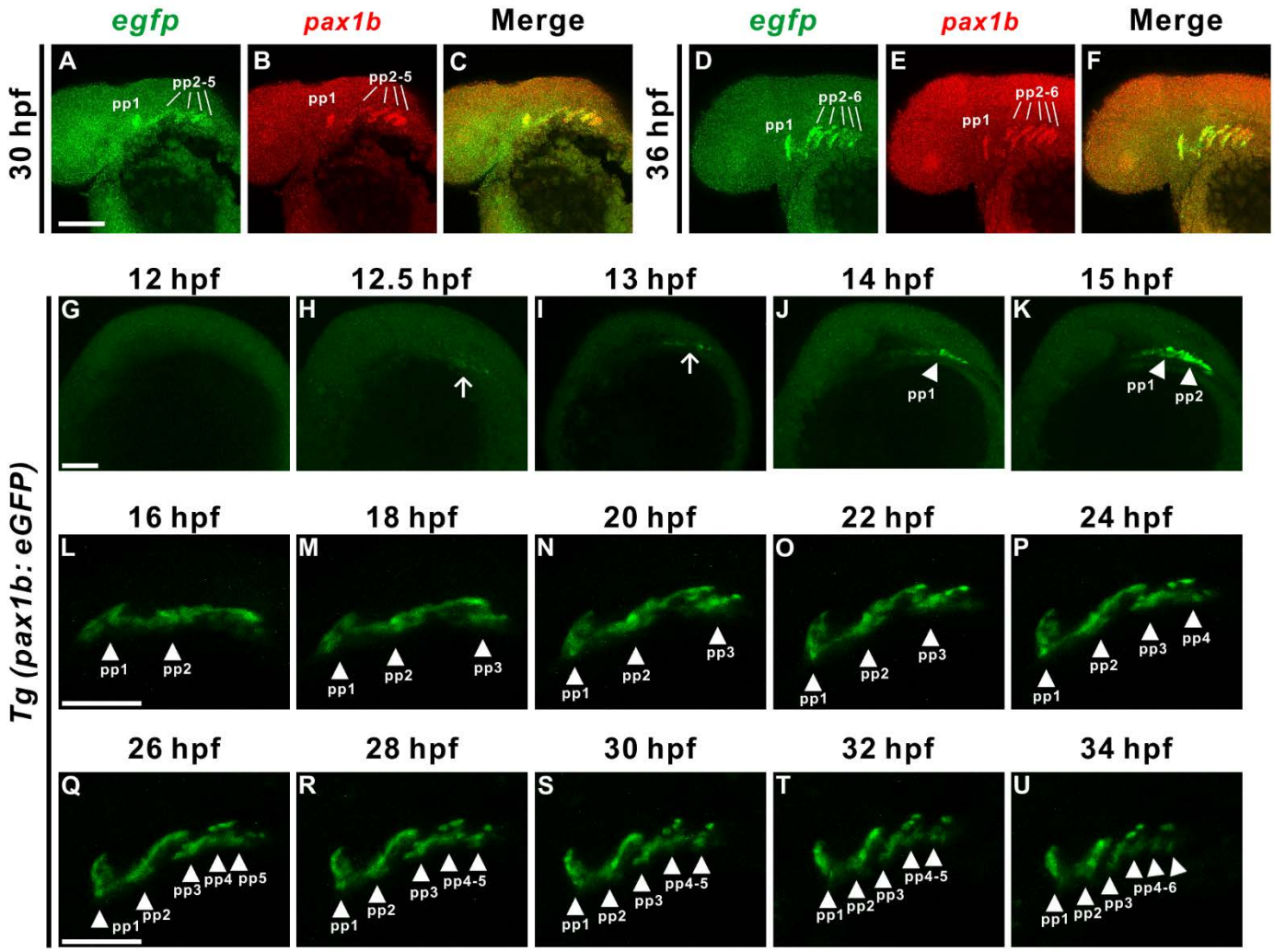

Fig. 6. Time lapse analyses of *Tg(pax1b:eGFP)* enhancer trap transgenic embryos reveals sequential segmental development of pharyngeal pouches.

Double fluorescence *in situ* hybridization indicated co-expression of *egfp* (A, D, green) with *pax1b* (B, E, red) in pharyngeal pouches (pp) 1-5 or 1-6 (C, F, merge) at 30 and 36 hpf. Time lapse analyses of *Tg(pax1b:eGFP)* transgenic embryos show morphogenesis of pharyngeal pouch 1-6 during 12 to 34 hpf stages. Lateral view of a *Tg(pax1b:eGFP)* embryo at 12 hpf (G), 12.5 hpf (H), 13 hpf (I), 14 hpf (J), 15 hpf (K), 16 hpf (L), 18 hpf (M), 20 hpf (N), 22 hpf (O), 24 hpf (P), 26 hpf (Q), 28 hpf (R), 30 hpf (S), 32 hpf (T) and 34 hpf (U) are shown. Scale bars represent 100 μm.

doi:10.6342/NTU202000783

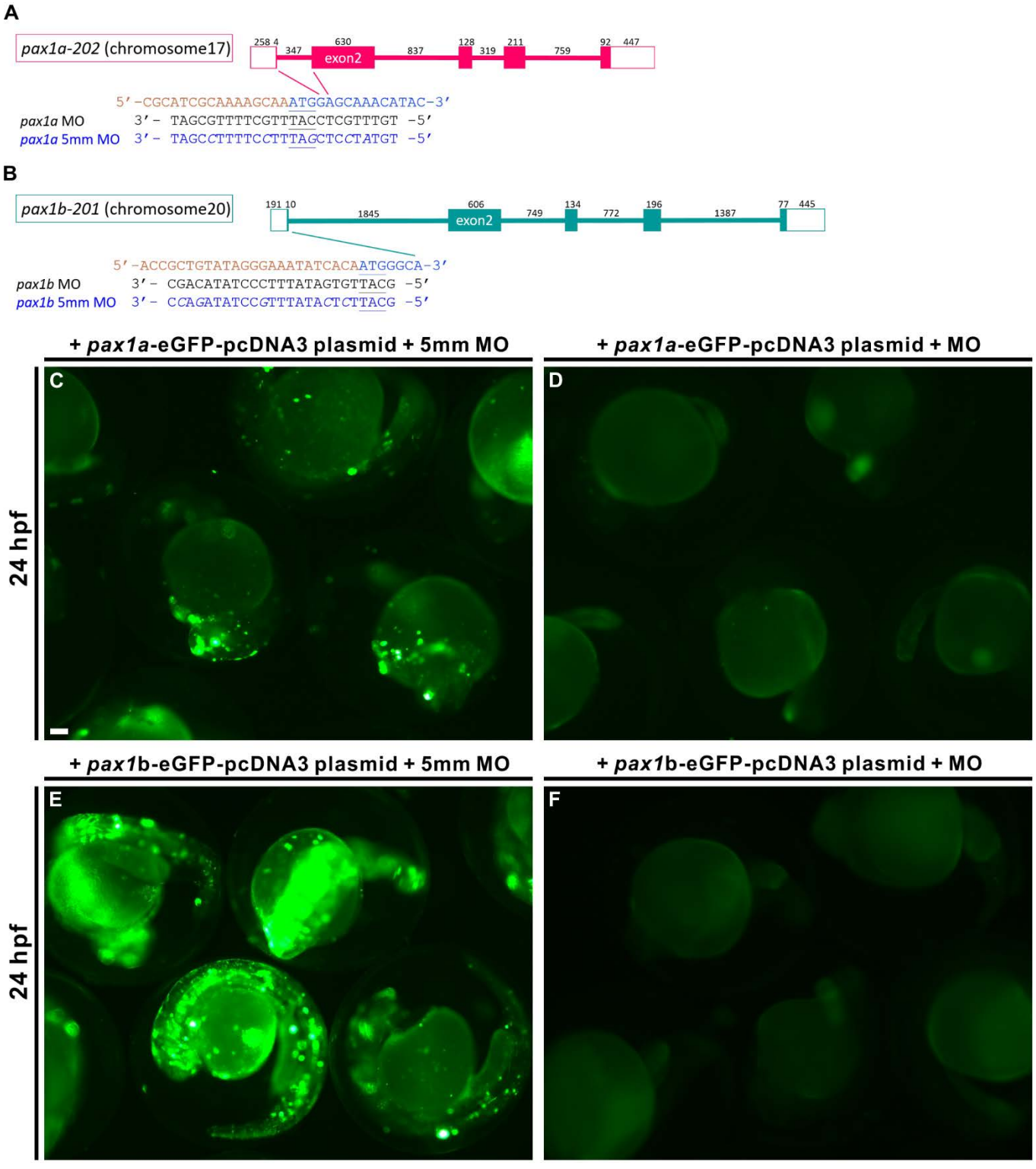

doi:10.6342/NTU202000783

Fig. 7. Specificity evaluation of *pax1a* MO and *pax1b* MO. (A) Sequences of *pax1a* MO and*pax1a* 5mm MO as well as complementary *pax1a* mRNA sequence are shown . (B) Sequences of *pax1b* MO and *pax1b* 5mm MO as well as complementary *pax1b* mRNA sequence are shown. (C, E) eGFP green fluorescence is detected in embryos co-injected with *pax1a-eGFP-pcDNA3* or *pax1b-eGFP-pcDNA3* plasmid and respective *pax1a* or *pax1b* 5mm MO at 24 hpf. (D, F) No eGFP expression can be observed in the majority of embryos co-injected with *pax1a-eGFP-pcDNA3* or *pax1b-eGFP-pcDNA3* plasmid and respective *pax1a* or *pax1b* MO.

doi:10.6342/NTU202000783

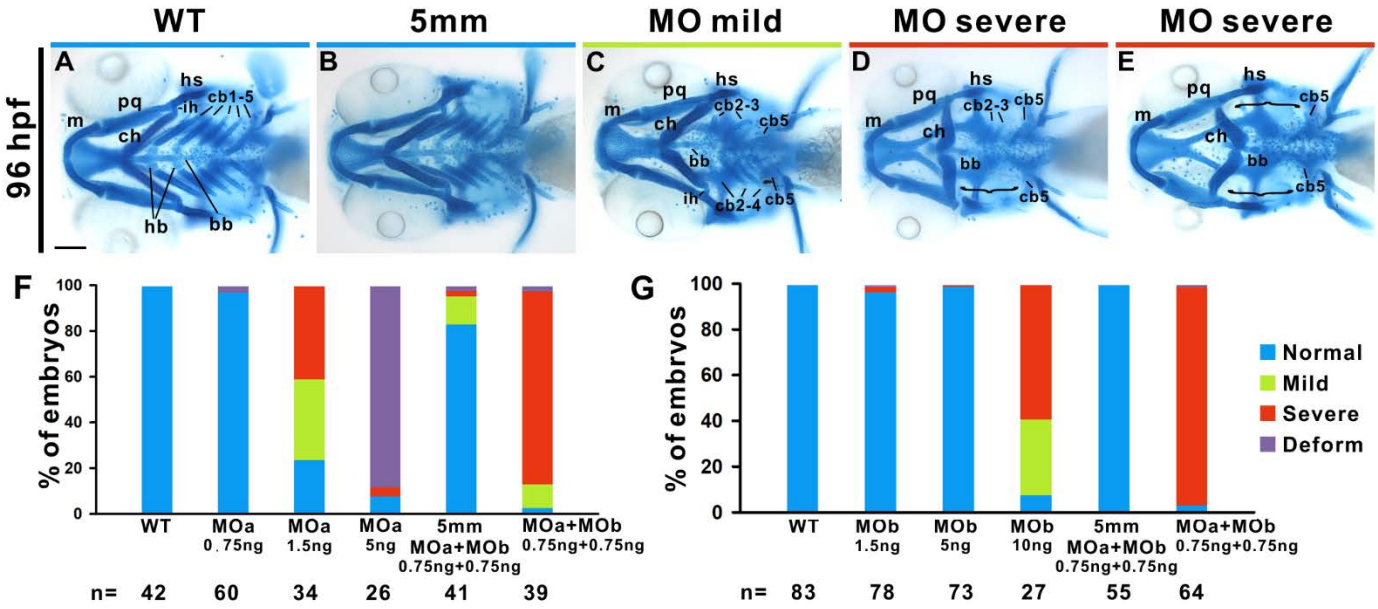

Fig. 8. Pax1a and Pax1b are redundant in regulating pharyngeal cartilage development. Mandibular pharyngeal arch 1 (Meckel's cartilage (m) and palatoquadrate (pq)), hyoid pharyngeal arch 2 (hyosymplectic (hs), interhyal (ih), ceratohyal (ch)) and five branchial arches (ceratobranchial (cb), hypobranchial (hb) and basibranchial (bb)) were identified in Alcian blue-stained wild type (A) and embryos injected with 0.75 ng each of 5mm *pax1a* MO and 5mm *pax1b* MO (B) at 96 hpf are shown. Mild pharyngeal cartilage defect (C, shortened cb 2-3, lack of cb 1 and 4 on one side and lack of cb1 on the other side) and two types of severe cartilage defects (D, straightened ch, shortened cb 2-3, lack of cb 1 and 4 on one side and lack of cb1-4 on the other side; E, reversed ch and lack of cb 1-4 on both sides) were detected in respective embryos injected with 1.5 ng *pax1a* MO (MOa), 10 ng *pax1b* MO (MOb), or 0.75 ng of both *pax1a* MO and *pax1b* MO. The majority of embryos injected with suboptimal dose (0.75 ng) of both *pax1a* MO and *pax1b* MO exhibited severe pharyngeal cartilage defects, while embryos injected with 1.5 ng *pax1a* MO or 10 ng *pax1b* MO showed less frequent severe phenotypes (F, G). Number of embryos for various treatment is shown under the x -axis. Brackets indicate lack of cb1-4. Scale bar represents 100 μm.

doi:10.6342/NTU202000783

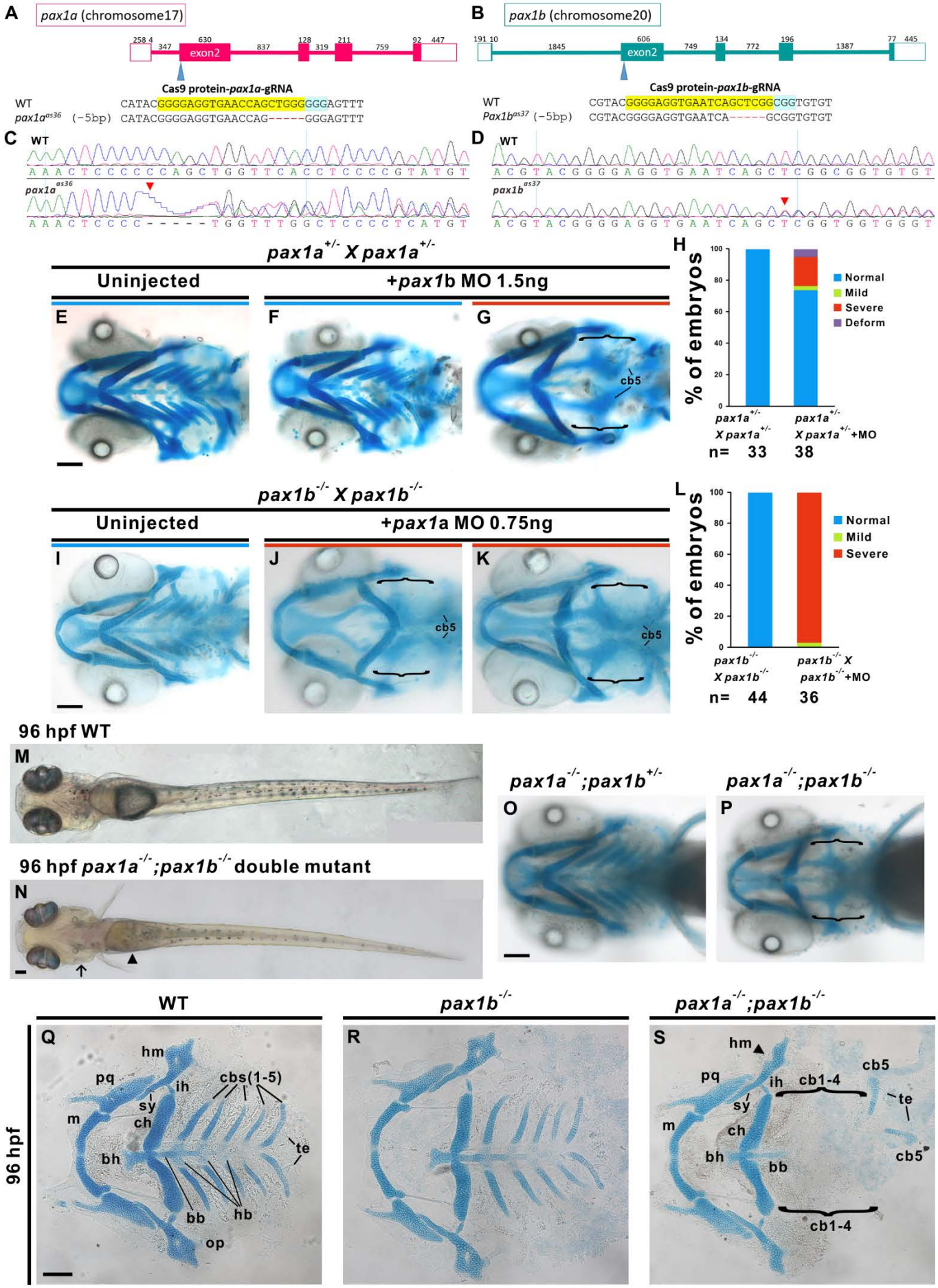

doi:10.6342/NTU202000783

Fig. 9. *pax1a*- and *pax1b*-deficient embryos generated by CRISPR-Cas9 mutagenesis exhibit abnormality of hyoid cartilage and lack of ceratobranchial cartilages 1-4. Genomic structures of *pax1a* (A) and *pax1b* (B) include the target sites for *pax1a* sgRNA and *pax1b* sgRNA in exon 2 of each gene. Nucleotide sequence of wild type (WT) and sequences of $pax1a^{as36}$ and $pax1b^{as37}$ mutants containing 5-bp deletions (red dashed line) are shown (A, B). sgRNA sequence (yellow highlight) and protospacer adjacent motif (PAM, blue highlight) are indicated. (C, D) Sequences of WT and $pax1a^{as36}$ or $pax1b^{as37}$ mutants were compared. Positions of deleted sequences in $pax1a^{as36}$ or $pax1b^{as37}$ mutants are indicated by arrowheads. Normal patterning of pharyngeal arches was detected in Alcian blue-stained uninjected (E) or 1.5 ng *pax1b* MO-injected $pax1a^{+/-}$ incrossed embryos (F) at 96 hpf. About 21.1% of $pax1a^{+/-}$ incrossed embryos that had been injected with 1.5 ng *pax1b* MO failed to develop ceratobranchial cartilages (G, H). Similarly, normal pharyngeal cartilage development was identified in Alcian blue-stained uninjected $pax1b^{-/-}$ incrossed embryos (I) while loss of ceratobranchial cartilage and hyoid cartilage with inverted (J) or no (K) anterior-posterior polarity were detected in 0.75 ng *pax1a* MO-injected $pax1b^{-/-}$ incrossed embryos stained with Alcian blue at 96 hpf. A comparison of the percentage embryos with pharyngeal cartilage defects in uninjected and *pax1a* MO-injected $pax1b^{-/-}$ incross embryos is shown (L). A $pax1a^{-/-}$; $pax1b^{-/-}$ double mutant embryo (N) exhibits a straight body, lack of swim bladder (arrowhead) and lack of gill cartilages (arrow), in contrast with wild type (M) at 96 hpf. Alcian blue-stained $pax1a^{-/-}$; $pax1b^{-/-}$ double mutant embryo (P) has no ceratobranchial cartilage, in contrast with $pax1a^{-/-}$; $pax1b^{+/-}$ mutant embryo (O) with normal pharyngeal cartilages at 96 hpf. Flat mount Alcian blue staining of pharyngeal cartilage revealed loss of ceratobranchial (cb) cartilages 1-4 with retention of shorter cb cartilage 5 in $pax1a^{-/-}$; $pax1b^{-/-}$ double mutants. Basibranchial (bb) cartilages 2-5 were also absent, with retention of bb cartilage 1. All hypobranchial (hb) cartilages and anterior hyomandibula (hm, arrowhead) were also absent in $pax1a^{-/-}$; $pax1b^{-/-}$ double mutants (S) in contrast to wild type (Q) and $pax1b^{-/-}$ mutant embryos (R) at 96 hpf. Brackets indicate lack of cb1-4. Ch, ceratohyal; ih, interhyal; m, Meckel's cartilage; op, opercular bone; pq, palatoquadrate; sy, symplectic; te, teeth. Scale bars represent 100 μm.

doi:10.6342/NTU202000783

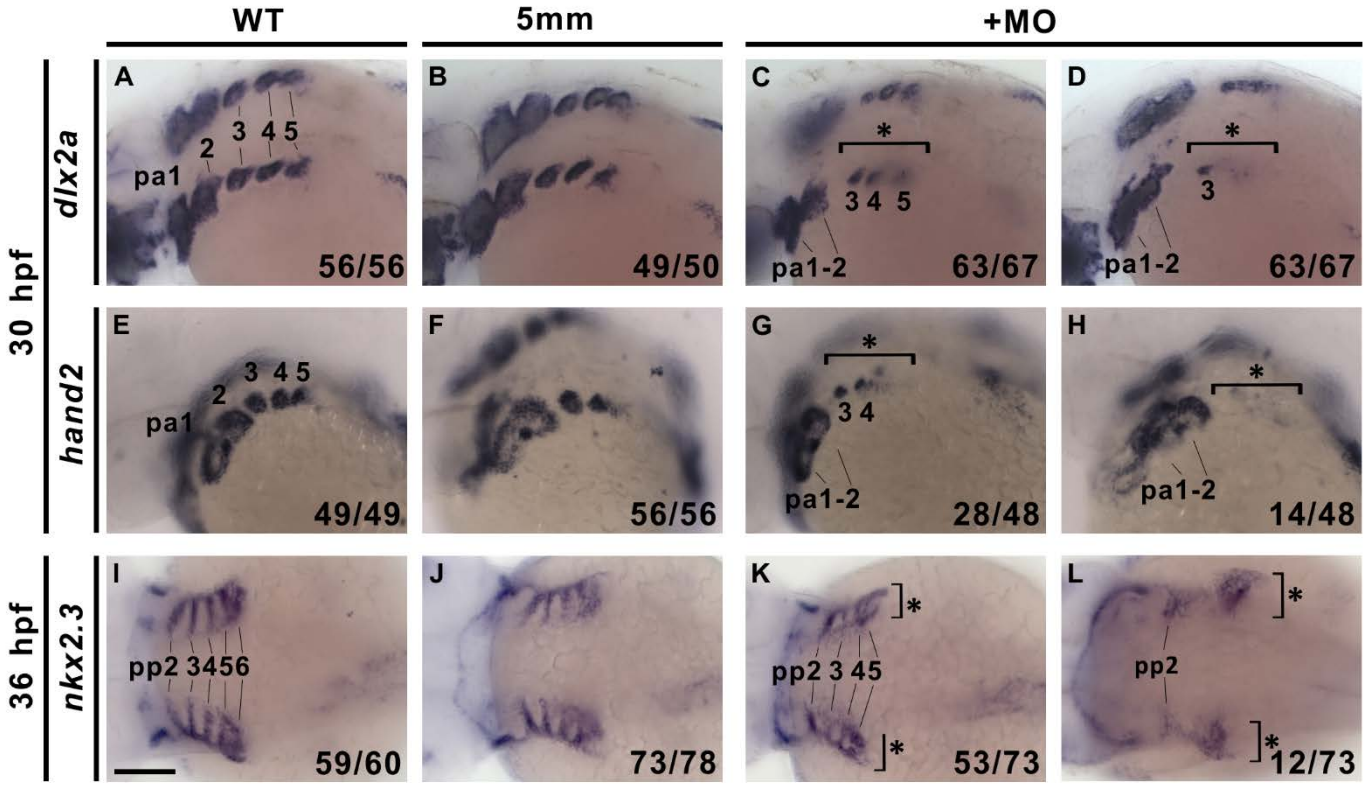

Fig. 10. Knockdown of *pax1a* and *pax1b* decreases expression of neural crest markers *dlx2a* or *hand2* or endodermal pouches marker *nkx2.3*. Reduced *dlx2a* expression (C, D) is detected in 3-5 pharyngeal arches in *pax1a*; *pax1b* morphant embryos compare with WT (A) and 5mm control (B) at 30 hpf. Reduced (G) or absent (H) of *hand2* expression are observed in 3-5 pharyngeal arches of *pax1a*; *pax1b* morphant embryos compare with WT (E) and 5mm control (F) at 30 hpf. Abnormal (K) and partial absent (L) *nkx2.3* expression pattern is detected in *pax1a*; *pax1b* morphant at 36 hpf. Asterisks indicate reduced or absent expression. Affected embryos per total number of analyzed embryos are shown. Scale bars represent 100 μm.

doi:10.6342/NTU202000783

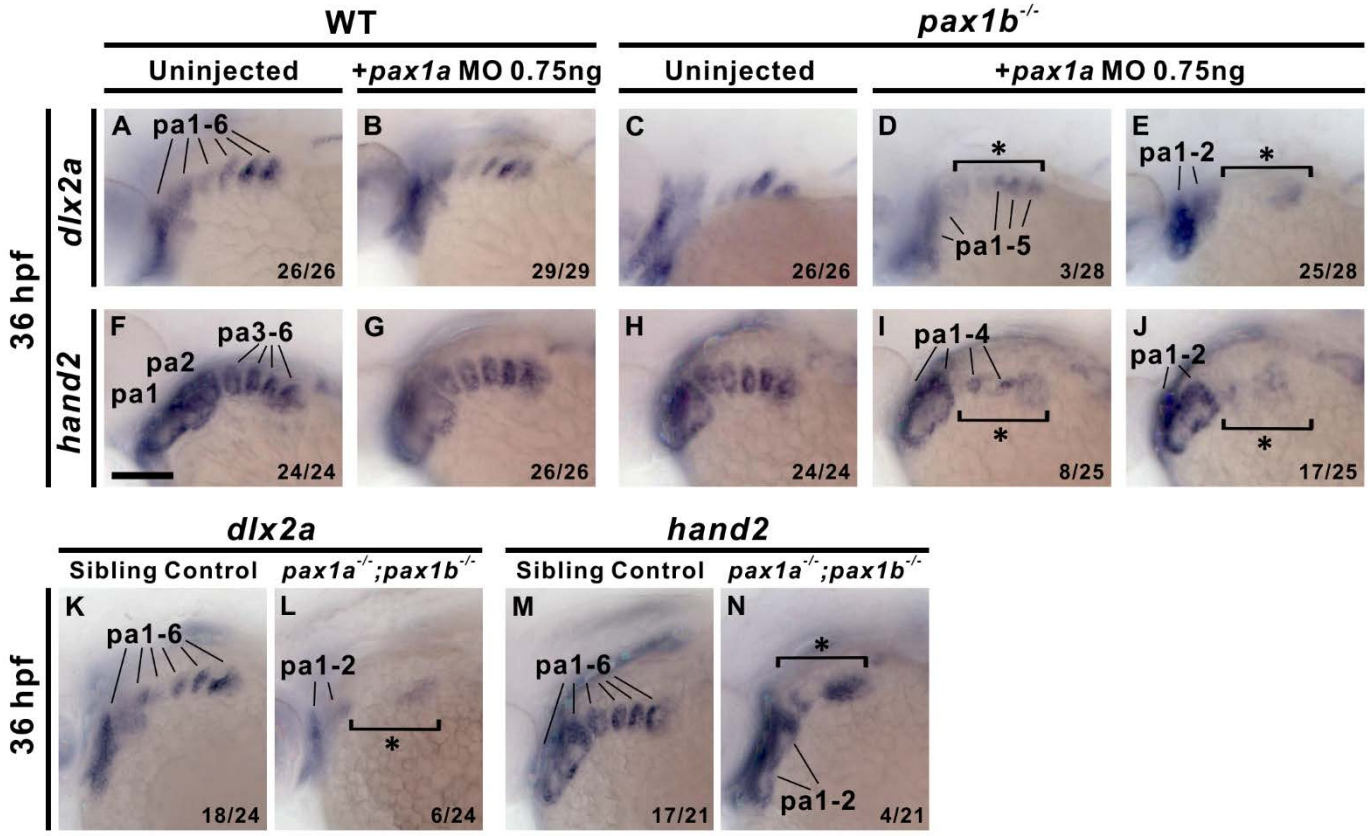

Fig. 11. *pax1a*- and *pax1b*-deficient embryos display decrease or absence of *dlx2a* and *hand2* expression in pharyngeal arches. Reduced expression of *dlx2a* (D) or *hand2* (I) as well as absence of *dlx2a* (E) or *hand2* (J) in the posterior pharyngeal arches (pa) was identified in 0.75 ng *pax1a* MO-injected *pax1b*$^{-/-}$ mutant embryos compared to uninjected *pax1b*$^{-/-}$ mutant (C, H), wild type (WT; A, F) or 0.75 ng *pax1a* MO-injected wild type (B, G) at 36 hpf. Similar defects in expression of *dlx2a* (L) or *hand2* (N) in the posterior pharyngeal arches were also identified in *pax1a*$^{-/-}$; *pax1b*$^{-/-}$ double mutants compared with sibling controls (i.e., *pax1a*$^{+/-}$; *pax1b*$^{-/-}$ or *pax1a*$^{+/+}$; *pax1b*$^{-/-}$) (K, M) at 36 hpf. Asterisks indicate reduced or absent expression. Affected embryos per total number of analyzed embryos are shown. Scale bars represent 100 μm.

doi:10.6342/NTU202000783

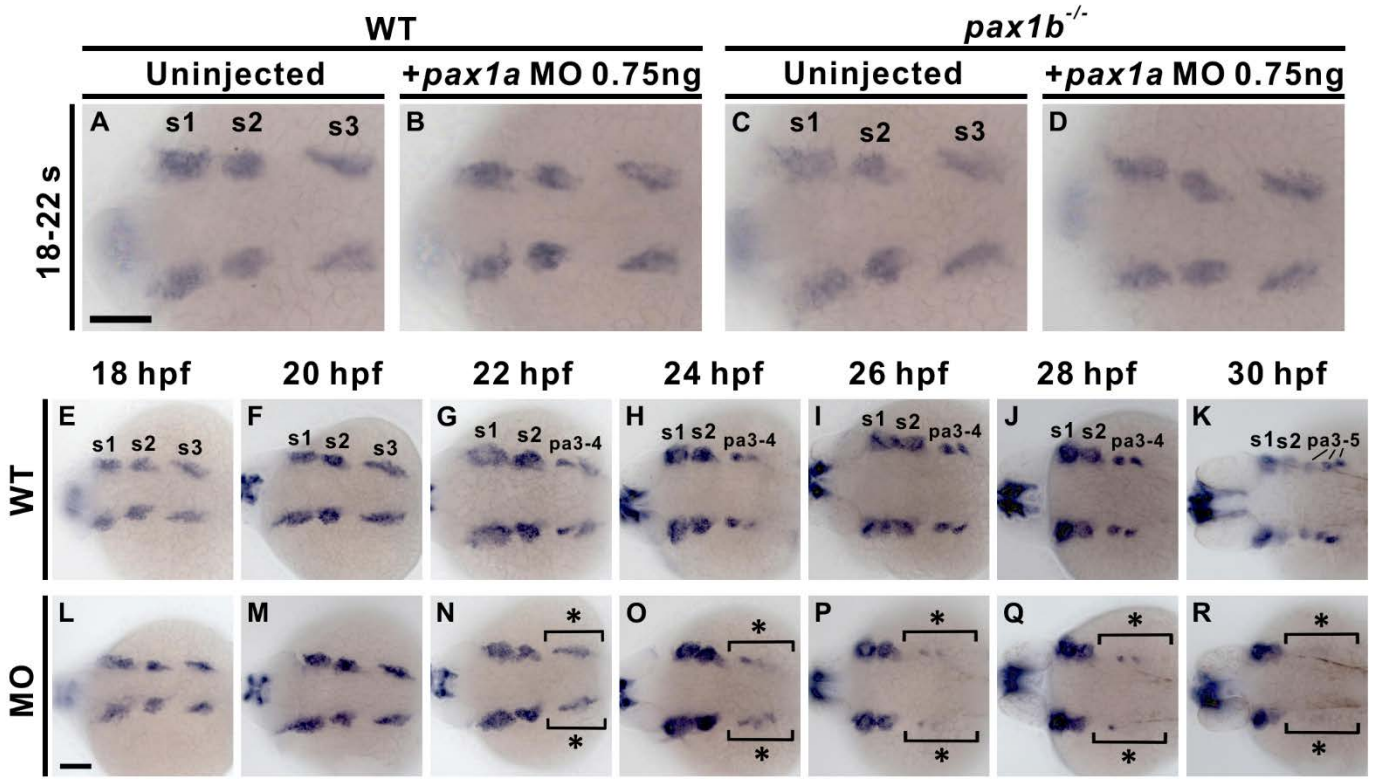

Fig. 12. Reduced *dlx2a* expression in pharyngeal arches 3-4 in *pax1a*; *pax1b* morphants beginning at 22 hpf. Reduced *dlx2a* expression in pharyngeal arches 3-4 in *pax1a*; *pax1b* morphants beginning at 22 hpf. Similar *dlx2a* expression levels were detected in three migrating streams (S1, S2, S3) of cranial neural crest cells in uninjected (C), 0.75 ng *pax1a* MO-injected *pax1b*$^{-/-}$ mutant embryos (D), uninjected wild type (WT; A) or 0.75 ng *pax1a* MO-injected wild type (B) during 18-22 s stages. Similar *dlx2a* expression levels in three migrating streams of cranial neural crest cells were observed in wild type and *pax1a*; *pax1b* morphants at 18 hpf (E, L) and 20 hpf (F, M). However, reduced *dlx2a* expression (asterisk) was identified in pharyngeal arches (pa) 3-4 of *pax1a*; *pax1b* morphants compared to wild type embryos at 22 hpf (G, N), 24 hpf (H, O), 26 hpf (I, P), 28 hpf (J, Q) and 30 hpf (K, R). Scale bars represent 100 μm.

doi:10.6342/NTU202000783

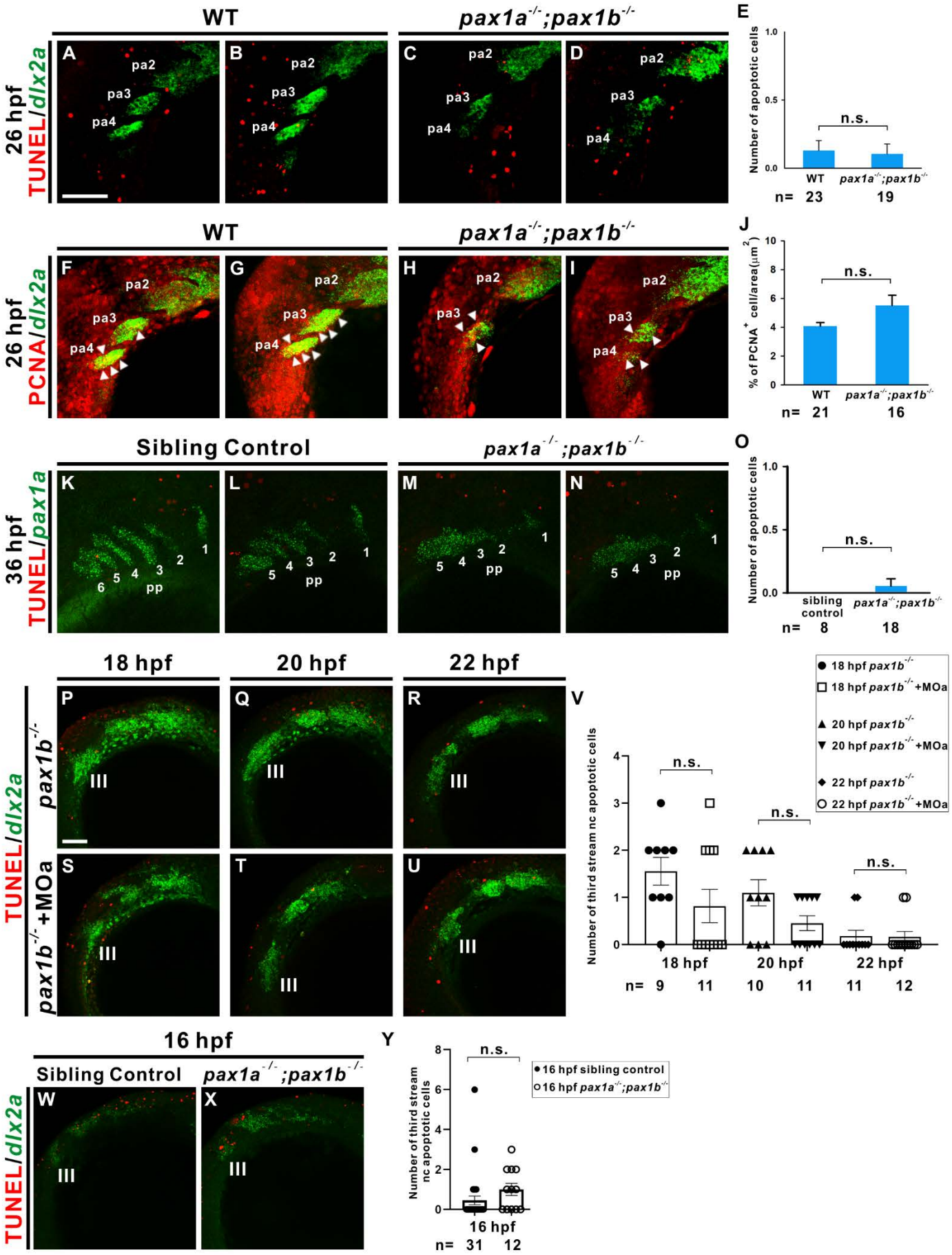

doi:10.6342/NTU202000783

Fig. 13. Similar levels of apoptosis and proliferation were observed in *pax1a*- and *pax1b*-deficient embryos. TUNEL assay was performed in wild type (WT) (A, B) and *pax1a*$^{-/-}$; *pax1b*$^{-/-}$ double mutant (C, D) embryos that were hybridized with *dlx2a* antisense RNA at 26 hpf. Quantification of apoptotic cells in pharyngeal arches (pa) 3 and 4 in wild type and mutant is shown (E). Proliferation was evaluated by anti-PCNA antibody in wild type (F, G) and *pax1a*$^{-/-}$; *pax1b*$^{-/-}$ double mutant (H, I) embryos that were hybridized with *dlx2a* antisense RNA at 26 hpf. Quantification of proliferation rate in pharyngeal arches 3 and 4 in wild type and mutant is shown (J). TUNEL assay was performed in sibling control (i.e., *pax1a*$^{+/-}$; *pax1b*$^{-/-}$ or *pax1a*$^{+/+}$; *pax1b*$^{-/-}$) (K, L) and *pax1a*$^{-/-}$; *pax1b*$^{-/-}$ double mutant (M, N) embryos that were hybridized with *pax1a* antisense RNA at 36 hpf. Quantification of apoptotic cells in pharyngeal pouches (pp) 2-6 in sibling control and mutant is shown (O). TUNEL assays were conducted in uninjected *pax1b*$^{-/-}$ mutant (P-R) and 0 .75 ng *pax1a* MO-injected *pax1b*$^{-/-}$ incrossed embryos (S-U) that were hybridized with *dlx2a* antisense RNA at 18, 20 and 22 hpf. (V) Quantification of apoptotic cells in third stream of neural crests in uninjected *pax1b*$^{-/-}$ mutant and *pax1a* MO-injected *pax1b*$^{-/-}$ mutant embryos at these stages. Sibling control (W) and *pax1a*$^{-/-}$; *pax1b*$^{-/-}$ double mutant embryos (X) that were hybridized with *dlx2a* antisense RNA were evaluated for apoptosis by TUNEL assay at 16 hpf. (Y) Quantification of apoptotic cells in third stream of neural crests in sibling control and mutant is shown. Arrowheads indicate neural crest cells labeled with PCNA and *dlx2a*. Statistical significance was evaluated by Student's *t*-test, n. s., not significant. Error bars indicate standard error. Scale bar represents 100 μm.

doi:10.6342/NTU202000783

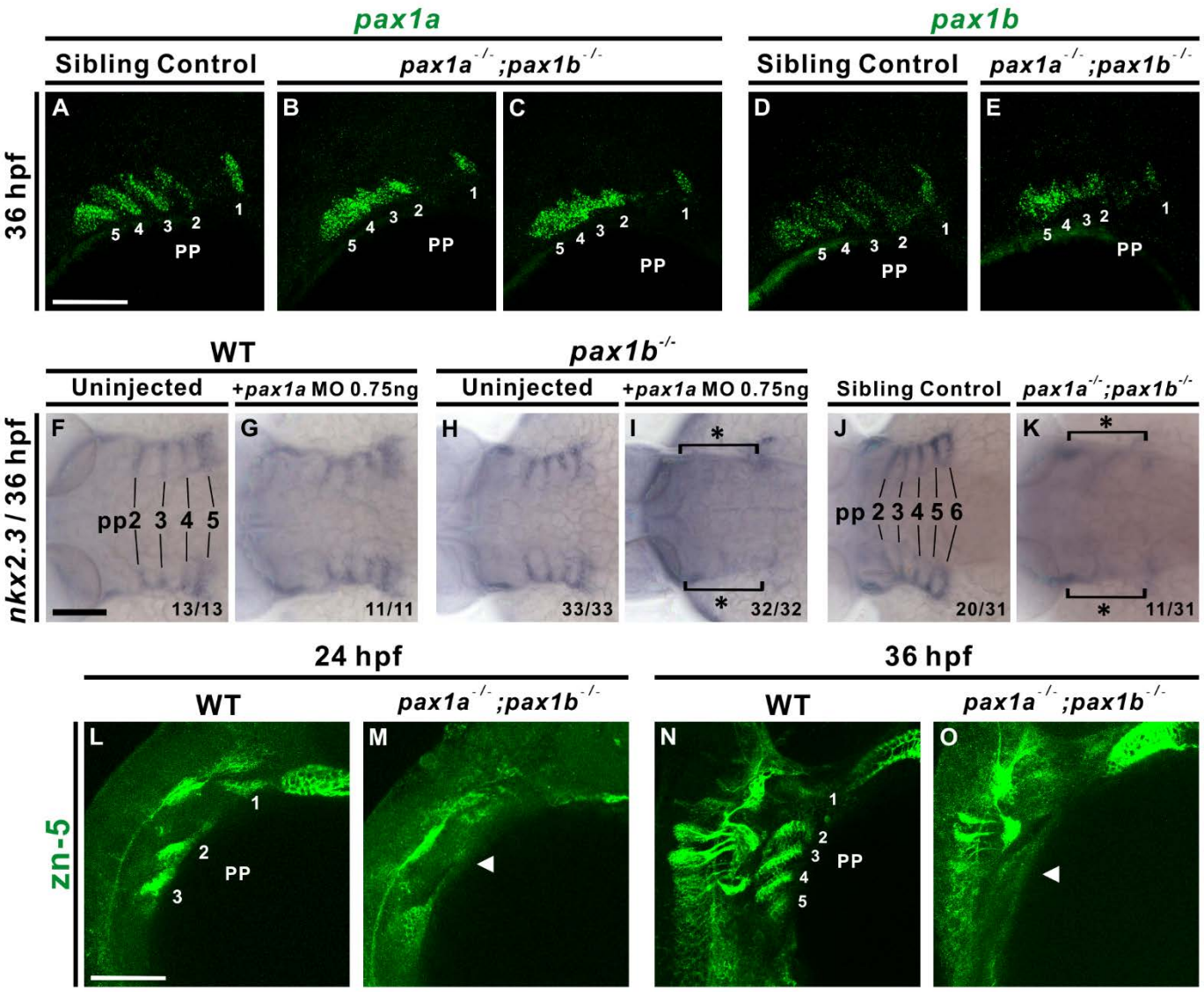

Fig. 14. *pax1a*- and *pax1b*-deficient embryos exhibit morphogenetic defects and lack of *nkx2.3* or Alcama expression in the pharyngeal pouches. Segmented pharyngeal pouch (pp) 1 expresses *pax1a* or *pax1b*, while unsegmented pharyngeal pouches 2-5 display continuous expression of *pax1a* or *pax1b* and small outpocketings in *pax1a*$^{-/-}$; *pax1b*$^{-/-}$ double mutant embryos (B, C, E); sibling controls (i.e., *pax1a*$^{+/-}$; *pax1b*$^{-/-}$ or *pax1a*$^{+/+}$; *pax1b*$^{-/-}$) show normal segmentation (A, D) when hybridized with *pax1a* or *pax1b* RNA probes at 36 hpf. Absent expression of *nkx2.3* in the pharyngeal pouches (pp) 2-5 was observed in 0.75 ng *pax1a* MO-injected *pax1b*$^{-/-}$ mutant embryos (I) compared to un-injected *pax1b*$^{-/-}$ mutants (H), wild types (WT; F) or 0.75 ng *pax1a* MO-injected wild types (G) at 36 hpf. A similar defect in *nkx2.3* expression in pharyngeal pouches 2-6 was also identified in *pax1a*$^{-/-}$; *pax1b*$^{-/-}$ double mutants (K) compared with sibling controls (i.e., *pax1a*$^{+/-}$; *pax1b*$^{-/-}$ or *pax1a*$^{+/+}$; *pax1b*$^{-/-}$) (J). A lack of Alcama expression (arrowhead; labeled by anti-zn5 antibody) was noted in the pharyngeal pouches of *pax1a*$^{-/-}$; *pax1b*$^{-/-}$ double mutants in contrast with wild types at 24 hpf (L, M) and 36 hpf (N, O). Scale bars represent 100 μm.

doi:10.6342/NTU202000783

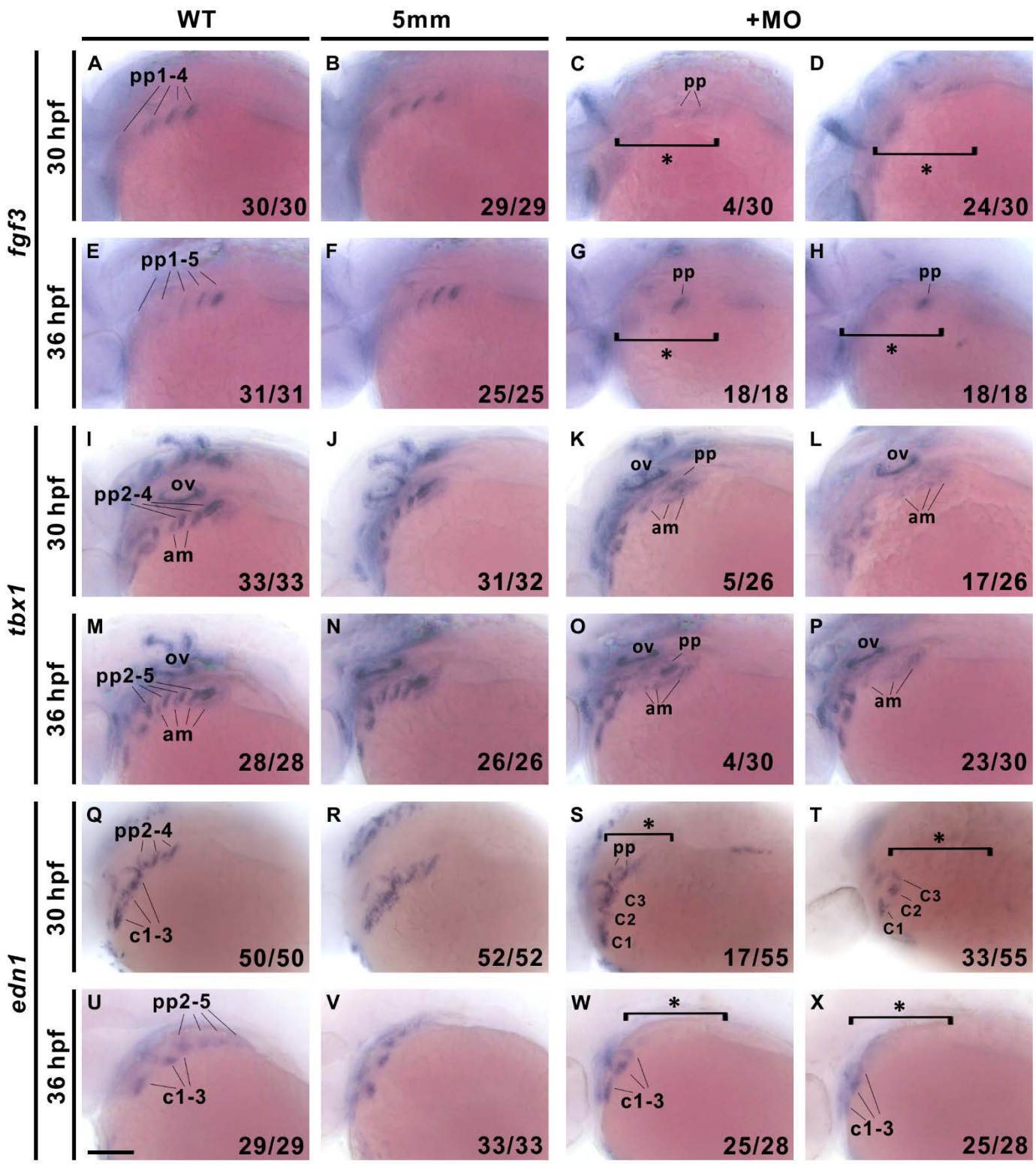

doi:10.6342/NTU202000783

Fig. 15. Reduced expressions of *edn1*, *fgf3*, or *tbx1* in pharyngeal pouches are detected in *pax1a*; *pax1b* morphant embryos. *fgf3* expression is reduced (C) or absent (D) in paryngeal pouches (pp) 1-4 in *pax1a*; *pax1b* morphant embryos compare to WT (A) and 5mm control (B) at 30 hpf. *fgf3* expression is absent (G, H) in paryngeal pouches 1-5 in *pax1a*; *pax1b* morphant embryos compare to WT (E) and 5mm control (F) at 36 hpf. *tbx1* expression is reduced (K, O) or absent (L, P) in paryngeal pouches 2-4 or 2-5 in *pax1a*; *pax1b* morphant embryos compare to WT (I, M) and 5mm control (J, N) at 30 and 36 hpf. *edn1* expression is reduced (S) or absent (T, W, X) in paryngeal pouches 2-4 or 2-5 in *pax1a*; *pax1b* morphant embryos compare to WT (Q, U) and 5mm control (R, V) at 30 and 36 hpf. Asterisks or arrowheads indicate reduced or absent expression. Affected embryos per total number of analyzed embryos are shown. Am, adjacent mesoderm; c, mesodermal core; ov, otic vesicle. Scale bars represent 100 μm.

doi:10.6342/NTU202000783

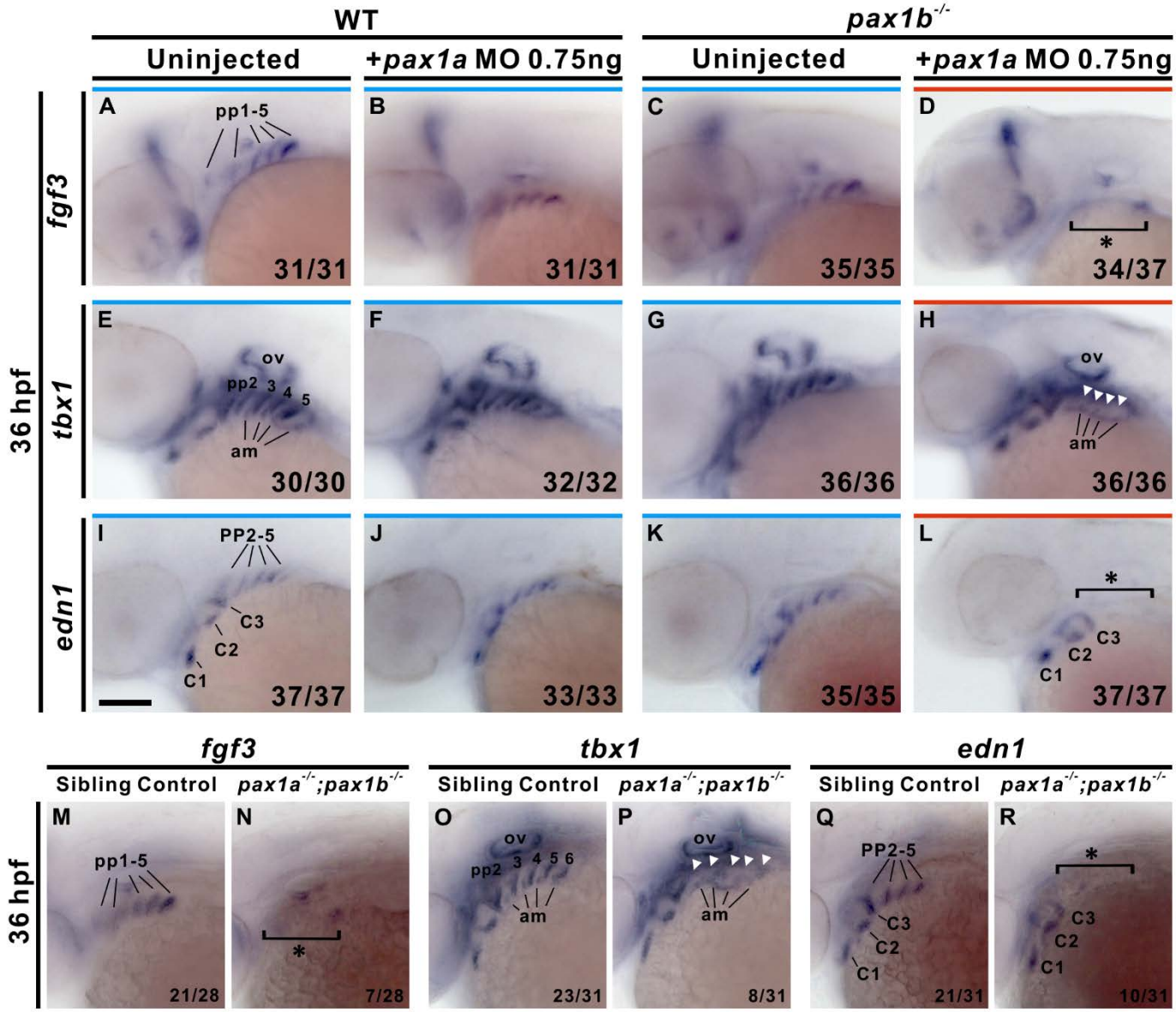

Fig. 16. *pax1a*- and *pax1b*-deficient embryos exhibit absent *fgf3*, *tbx1* and *edn1* expression in pharyngeal pouches. Absent expression of *fgf3* in pharyngeal pouches (pp) 1-5 was identified in 0.75 ng *pax1a* MO-injected *pax1b*$^{-/-}$ mutant embryos (D) compared to uninjected wild type (WT) (A), 0.75 ng *pax1a* MO-injected wild type (B) or uninjected *pax1b*$^{-/-}$ mutant embryos (C) at 36 hpf. Similar absent expression of *tbx1* or *edn1* in posterior pharyngeal pouches 2-5 were observed in 0.75 ng *pax1a* MO-injected *pax1b*$^{-/-}$ mutant embryos (H, L) compared to uninjected wild type (E, I), 0.75 ng *pax1a* MO-injected wild type (F, J) or uninjected *pax1b*$^{-/-}$ mutant embryos (G, K) at 36 hpf. Similar defects in endodermal expression of *fgf3* (N), *tbx1* (P) and *edn1* (R) in pharyngeal pouches were also found in *pax1a*$^{-/-}$; *pax1b*$^{-/-}$ double mutants in contrast with sibling controls (i.e., *pax1a*$^{+/-}$; *pax1b*$^{-/-}$ or *pax1a*$^{+/+}$; *pax1b*$^{-/-}$) (M, O, Q) at 36 hpf. Asterisks or arrowheads indicate absent expression. Affected embryos per total number of analyzed embryos are shown. Am, adjacent mesoderm; c, mesodermal core; ov, otic vesicle. Scale bars represent 100 μm.

doi:10.6342/NTU202000783

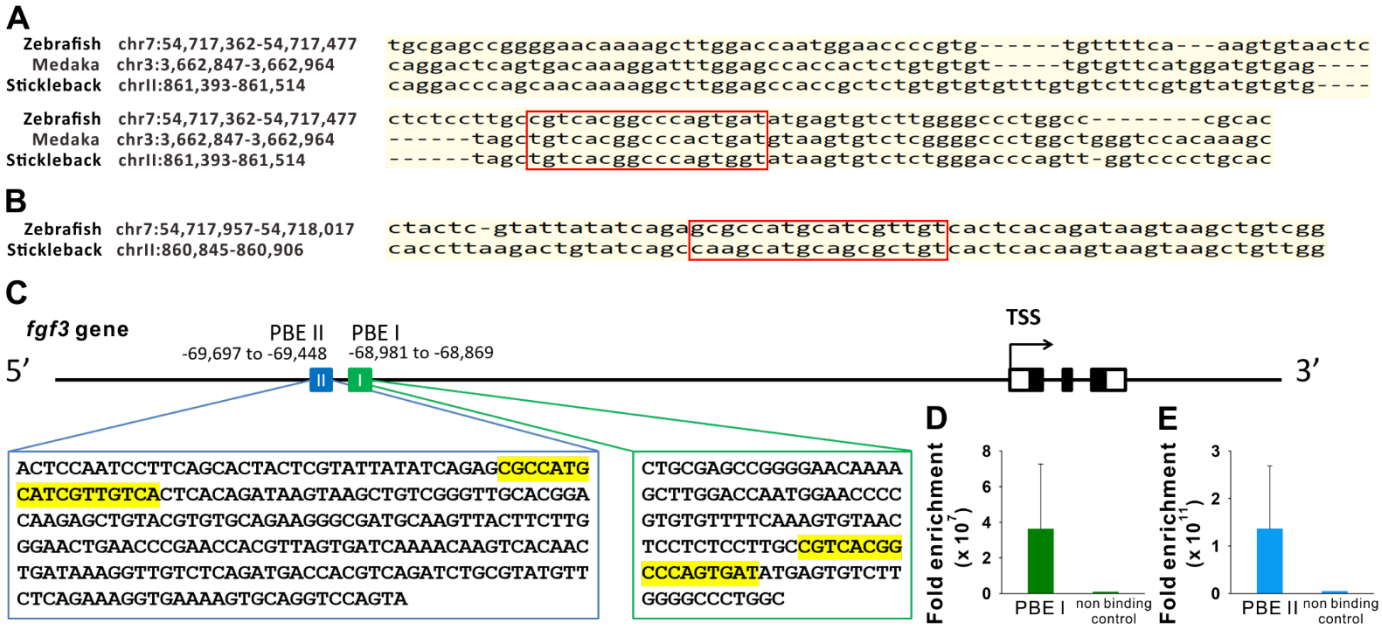

Fig. 17. Pax1b directly binds to PAX binding elements 5′ upstream of the *fgf3* gene. The UCSC genome browser search result revealed the location of conserved PAX binding element (PBE) I (A) or PBE II (B) in zebrafish, medaka and stickleback, or in zebrafish and stickleback. (C) The diagram illustrates the nucleotide sequence surrounding PBE I and PBE II, which are located 5′ upstream of the *fgf3* gene. Significantly enriched PCR product was derived from chromatin precipitated by anti-Myc antibody compared to anti-IgG antibody or non-binding control, using primers for PBE I (D) or PBE II (E). TSS, transcription start site. Error bars indicate standard error.

doi:10.6342/NTU202000783

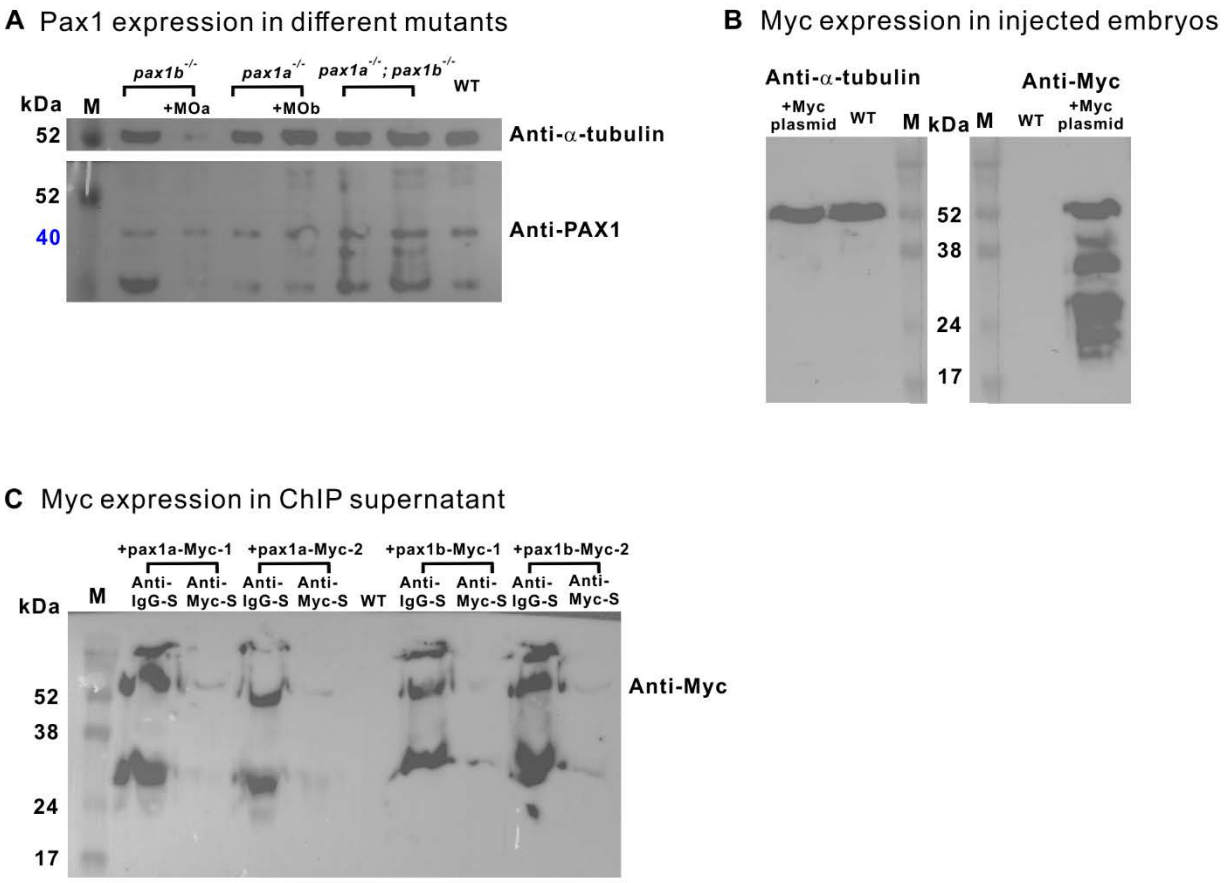

Fig. 18. Western blot for Pax1 and Myc-Pax1 expression. (A) Total protein isolated from *pax1b*$^{-/-}$ mutant, *pax1a* MO-injected *pax1b*$^{-/-}$ mutant, *pax1ba*$^{-/-}$ mutant, *pax1b* MO-injected *pax1a*$^{-/-}$ mutant, *pax1a*$^{-/-}$; *pax1b*$^{-/-}$ double mutant and wild type, embryos at 72 hpf were subjected to SDS PAGE and Western blot analysis using Anti-PAX1 antibody. Anti-α-tubulin antibody was used as internal control. (B) Total protein isolated from 36 hpf embryos injected with *pax1a*-Myc and *pax1b*-Myc plasmid were subjected to SDS PAGE and Western blot analysis using anti-Myc antibody. Anti-α-tubulin antibody was used as internal control. (C) Supernatants of ChIP using anti-Myc or anti-IgG antibody were subjected to SDS PAGE and Western blot analysis using anti-Myc antibody. M, molecular weight marker.

doi:10.6342/NTU202000783

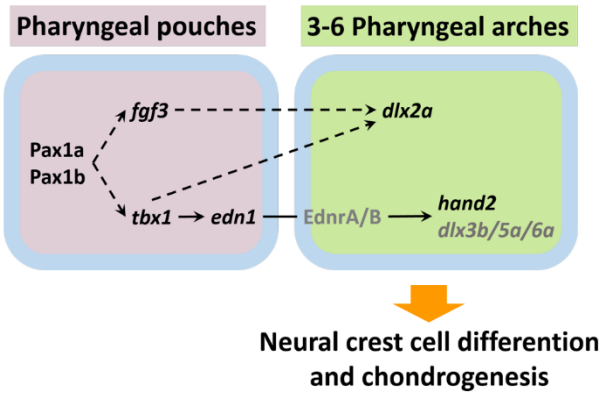

Fig. 19. A proposed model describing the function of Pax1a and Pax1b in regulating pharyngeal pouch morphogenesis and ceratobranchial cartilage formation. Pax1a and Pax1b act as an upstream integrator, modulating expression of *fgf3* and *tbx1* in pharyngeal pouches. Fgf3 signaling and Tbx1 then regulate *dlx2a* expression in the adjacent neural crest cells of pharyngeal arches 3-6, an essential action during neural crest cell differentiation and chondrogenesis. In pharyngeal pouches, Tbx1 also regulates expression of *edn1*, which then interacts with EdnrA/B in neural crest cells to modulate expression of downstream genes essential for neural crest differentiation and cartilage formation (i.e., *hand2*, *dlx3b*, *dlx5a*, and *dlx6a*).

doi:10.6342/NTU202000783

Publication list

1. **Liu YH**, Lin TC, Hwang SP. Zebrafish Pax1a and Pax1b are required for pharyngeal pouch morphogenesis and ceratobranchial cartilage development. Mechanisms of Development. 2020;161:103598.

2. Chen YC, Liao BK, Lu YF, **Liu YH**, Hsieh FC, Hwang PP, Hwang SP. Zebrafish Klf4 maintains the ionocyte progenitor population by regulating epidermal stem cell proliferation and lateral inhibition. PLOS Genet. 2019;15(4):e1008058.

3. Chang SS, Tu S, Baek KI, Pietersen A, **Liu YH**, Savage VM, Hwang SP, Hsiai TK, Roper M. Optimal occlusion uniformly partitions red blood cells fluxes within a microvascular network. PLOS computational biology. 2017;13(12):e1005892.

4. Lin CY, Tsai MY, **Liu YH,** Lu YF, Chen YC, Lai YR, Lien HW, Yang CH, Huang CJ, Hwang SP. Klf8 regulates left-right asymmetric patterning through modulation of Kupffer's vesicle morphogenesis and spaw expression. Journal of biomedical science. 2017;24(1):45.

5. Tsai MY, Lu YF, **Liu YH,** Lien HW, Huang CJ, Wu JL, Hwang SP. Modulation of p53 and met expression by Kruppel-like factor 8 regulates zebrafish cerebellar development. Developmental neurobiology. 2015;75(9):908-26.

doi:10.6342/NTU202000783